The Iraqi Journal for Mechanical and Material Engineering, Vol.42, No.1, May. 2025

EFFECT OF NANOFLUID/POROUS MEDIA VOLUME RATIO AND ROTATING CYLINDER ANGULAR VELOCITY ON MIXED CONVECTION FLUID FLOW INSIDE A SQUARE CAVITY WITH A WAVY BASE WALL HEAT SOURCE

Baraa H. Mahdi [1] **Rehab N. AL-kaby [2]**

baraahamzah2011@gmail.com **Eng.rehab.mohammed@uobabylon.edu.iq**

[1&2] Department of Mechanical Engineering, Engineering College of Babylon University, Babylon, Iraq.

ABSTRACT

In this study, a two-dimensional numerical method is employed to discretize the governing equations for heat transfer and mixed convection inside a square cavity with a sinusoidal bottom wall. The numerical method is based on the variational formulation/finite element with triangular nonsymmetrical elements. The vertical walls of the cavity are kept at a constant cold temperature, while the constant temperature heat source is applied to the sinusoidal bottom wall. The top wall and the rotating cylinder inside the cavity are considered insulated. The dimensionless angular velocities of an insulated rotating solid cylinder that have been considered are 0, 3000, and 6000 clockwise/counterclockwise. The working fluid is Al_2O_3 nanofluids with porous media at varying ratios. This analysis examined various ratios of nanofluids/porous media (nanoporous) volumes to the total enclosure volume, ranging from 0% to 100%, with a 25% increment. The effect of nanoporous media volume on the main pertinent parameters (velocity vector, heatlines, isotherms, dimensionless entropy, Bejan number, streamlines, and Nusselt numbers) is investigated at various solid cylinders' rotational angular velocities. A constant Rayleigh number (10^4), Darcy number (10^{-3}), and nanopartical solid volume fraction (0.02) are used. The results of the present work have been validated against several published works, to test the accuracy of the present analysis. In the present analysis, the data is plotted for different main parameters. The findings of this work showed that the average Nusselt number values on the hot wall increase as angular velocity increases, regardless of the rotational direction. Additionally, increasing the ratio of porous media/enclosure volume above 75% does not significantly impact the Nusselt number.

Keywords: Heatlines ,Mixed Convection, Nanofluid, Nanoporous, Wavy.

Received: December 6, 2024.

Accepted: March 25, 2025.

Nomenclature		**Greek characters**	
Amp	Dimensionless form of the Wavy Surface amplitude	ρ	Density (kg m^{-3})
Cp	A specific heat under constant pressure (J $kg^{-1}K^{-1}$)	β	The coefficient of thermal expansion (K^{-1})
Da	Darcy number, K/L^2	S_{gen}	Local entropy generation
g	Acceleration due to gravity (m s−2)	$\dot{S}$	Local entropy generation in all computational domains
HH	Nanoporous media height inside the cavity	Ϊ	Heat functions.
h	Local coefficient of heat transfer (W $m^{-2}K^{-1}$)	α	Thermal diffusivity (m^2 s^{-1})
K	Permeability of the porous medium (m^2)	ε	Porosity of porous media
k	Thermal conductivity (W m^{-1} K^{-1})	ν	Kinematic viscosity (m^2 s^{-1})
L_C	The enclosure's Characteristic length (m)	$\acute{\theta}$	Dimensionless form of temperature,
N	Amplitudes number		$\acute{\theta}$ =(T-T_c)/(T_h-T_c)
p	Pressure (N/m^2)	ϕ	Nanoparticle volume fraction
P	Dimensionless Pressure $(\frac{p}{\rho_f U_o^2})$	Ψ	Stream function
r	Radius of the inner cylinder (m)	ω	Inner cylinder rotational speed(rad s^{-1})
R	Dimensionless form of the inner cylinder radius R=r/Lc	Ω	Dimensionless form of rotational speed of the cylinder, $\Omega = \omega L_C^2/\alpha f$
T	Temperature (K)	μ	Dynamic viscosity (N.s.m^{-2})
$\acute{U}_o$	Linear velocity,$\acute{U}_o = \omega r$	μ_{nf}	Nanofluid dynamic viscosity (N.s.m^{-2})
ú , ý	components of Velocity (ms^{-1})	μ_f	Base fluids dynamic viscosity (N.s.m^{-2})
Ú,Ý	Dimensionless components of velocities, Ý = ý/ $Ú_o$, Ú = ú /$Ú_o$	**Subscripts**	
		nf,p	Nanofluid and porous medium
x, y	Dimensional coordinates (m)	c,h	Cold, Hot
X,Y	Dimensionless coordinates, X= x/LC, Y= y/LC	f	Base fluid
		gen	Generation
Dimensionless numbers		gen,T	Generation due to temperature effect
Be	Bejan number, $B_e = \frac{\dot{S}_{gen,T}}{\dot{S}_{gen}}$	gen, μ	Generation due to viscous dissipation
Gr	Grashof number, $Gr = g\beta f (Th-Tc) (L_c)^3 / \nu_f$	nf	Nanofluid
Nu_L	Local Nusselt number, Nu = h Lc/kf	np	Nanoparticle
$\overline{Nu}$	Mean Nusselt number	o	Cavity center, standard conditions
Pr	Prandtl number, Pr= νf /αf	p	Porous
Ra	Rayleigh number, $g\beta f(Th - Tc)L_C^3 / \nu f\alpha f$		
Re	Reynolds number, $Re = U_o L/\nu f$		
Ri	Richardson number, $Ri= Gr/Re^2$		

INTRODUCTION

The heat transfer by convection is one of the most crucial heat transfer processes that researchers focus on, and it is widely used in numerous applications, including water boiling, atmospheric warming, and solar heaters, (Lin et al., 2022, Sivasankaran and Mallawi, 2021, Vengadesan and Senthil, 2020). The convection heat transfer can be divided into two categories: free or natural convection, which is caused by buoyant forces, and forced convection, which take place when fluid flow is influenced by external sources like a pump or fan. To improve the system's thermal efficiency, most researchers study free convection because it has a lower heat transfer coefficient and there is no external source that can be adjusted to increase the heat transfer efficiency as in forced convection heat transfer, which makes free convection less costly than forced convection and no operating issues(Al-Asad et al., 2021, Bashir et al., 2019, Ghalambaz et al., 2020, Mehryan et al., 2020).

In certain applications, the heat process can be influenced by buoyant forces, inertial forces, and viscous forces at different degrees. This process is known as mixed convection because it involves both forced and free convection mechanisms at the same time. These applications include thermal storage unit design, solar collectors, journal-bearing lubrication, nuclear reactors, fuel rods, cooling of electronic equipment, drilling of oil wells, and heat exchangers(Abderrahmane et al., 2022, Ahmed et al., 2021, Ghorbani et al., 2010, Hatami et al., 2021, Hrairi et al., 2010, Isede and Adeniyan, 2021, Lipiński et al., 2021). Researchers have explored various techniques to improve heat transfer in cavities. These strategies include manipulating heating positions with discrete heaters (Rashid et al., 2023) inducing motion in one or more enclosure walls (Zheng et al., 2013), employing fixed or rotating objects (Selimefendigil et al., 2017), modifying the enclosure geometry(Aberoumand and Jafarimoghaddam, 2016), and utilizing fins or baffles. Enhance the thermophysical properties of the typical fluid by adding a nanoparticle, known as nanofluids, which is one of the most productively ways to improve the heat rate within cavities. Nanoparticles typically range in diameter from 1 to 100 nm (Bellos et al., 2018, Cherkasova and Shan, 2008, Trisaksri and Wongwises, 2007, Yazdanifard et al., 2017) and consist of different types of metallic and non-metallic materials (Ahmed et al., 2019, Das et al., 2006), such as Al_2O_3, CuO, TiO_2, TiC, SiC, Fe, Cu, Ag, Au, ..etc. (ÖZERİNÇ, 2010, Vakili et al., 2013, Yazdanifard et al., 2017). Several studies have been performed in nanoparticles shape and size such as (Dadwal and Joy, 2020, Ghaffarkhah et al., 2020, Maheshwary et al., 2020, Sharifi et al., 2020, Trodi and Benhamza, 2016, Xie et al., 2002, Zahmatkesh et al., 2021a, Zahmatkesh et al., 2021b). (Hatami et al., 2021) deduced that the heat transfer improves by rising the volume percentage of nanoparticles. They also noted that nano-rod alumina shows better heat transfer performance and Nusselt number compared to spherical alumina nanoparticles. (Tiwari and Das, 2007) analyzed the use of nanofluids for mixed convection inside enclosures. They studied the enhancement of heat rate in a lid-driven square cavity by adding nanoparticles. Their results showed that the average Nusselt number related with the solid volume fraction of the nanofluid in a nonlinear relationship.

(Misirlioglu, 2006) investigated mixed convection in a square enclosure filled with porous media. His results showed the forced convection regime is typically more influenced by the cylinder's rotation than the mixed convection regimes. Many studies have studied the whole effect of different cavity shapes on heat transfer and fluid flow under various boundary conditions.

The results have shown that the geometry of the cavity plays a critical role in heat transfer (Zafar et al., 2023). These geometries start from simple geometry like square enclosures with internal objects, curved tubes, rectangular shapes, and annular enclosures (Ahmed et al., 2020, Alam et al., 2012, Ali et al., 2018) to complicated shapes like H-shaped and trapezoidal cavities (Ali et al., 2020, Zhixiong Li, 2019). (Baïri et al., 2014) showed the influence of different enclosure shapes on the flow of fluid and heat rate under various boundary conditions, considering different heat source distributions and Rayleigh numbers. (Shih and Cheng, 2015) analyzed the influence of viscous dissipation on heat transfer inside cavities with different geometries, including squares, circles, and equilateral triangles with an adiabatic inner-revolving cylinder.

Recently, enclosures with a corrugated wall have been considered as another complex cavity shape that has attracted significant research interest. (Al-Amir et al., 2019) introduced a numerical analysis of the amplitude's effect and the undulations on a wavy surface on heat transfer. Their data demonstrated that increasing the surface amplitudes and undulation numbers at a constant Reynolds Number resulted in a heat transfer rate increasing.

(Zarei et al., 2022) studied the impact of a free convection inside a two-dimensional enclosure with a sinusoidal function wavy wall filled with Cu-Water nanofluid. They found that the Nusselt Number of the wavy wall increases as the wave amplitude increases.

In a study by (Alsabery et al., 2018), a numerical investigation was conducted on mixed convection in a wavy-walled square enclosure filled with Al_2O_3–water nanofluid with a rotating cylinder. They assumed that the side walls of the cavity were cooled and wavy. The top and bottom walls were insulated, they found that increasing the solid volume fraction improved the Nusselt number, and the revolving cylinder improved the heat rate for Rayleigh numbers less than $5 \times 10^{5.}$ Furthermore, the findings showed that the irreversibility due to temperature difference is dominant when the inner cylinder at rest. In contrast, when the cylinder rotates ($Be < 0.5$), the irreversibility controlled by nanofluid friction is the primary contributor.

Several researchers have studied and compared the impact of various cavity shapes on heat transfer. Recent studies have examined the saturation of porous media with nanofluids under various conditions, including changing geometries, considering different flow regimes, and using various boundary conditions and thermophysical characteristics(Jabbar et al., 2020, Khanafer and Vafai, 2018, Varol et al., 2009)**.**

The impact of porous medium on heat transfer rate was examed by (Prasad et al., 2017), using both numerical and experimental analysis. They conducted tests on a variable heat flux applied on vertical porous plate, using two types of nanofluids: silver (Ag) and copper (Cu) with water-based. The finding showed that the Cu-water nanofluid performs better than the other in terms of wall friction. Also, the fluid temperature drops with increasing heat source parameter values for both Cu-water and Ag-water nanofluids. (Hamdi et al., 2023) investigated heat transfer by convection in a vented square cavity with laminar flow. The porous media was filled with various nanofluids, such as Al_2O_3, Cu, Fe_3O_4, and Ag. The research demonstrated that the change of Reynolds and Darcy numbers infeluence the flow pattern and heat rate in the enclosure. Also, the heat rate rate in the enclosure is significantly influenced by the location and the thickness of the porous layer. Moreover, the Ag nanoparticles exhibited the highest thermal transfer rate compared to other nanoparticles.

This study yields results with broad practical implications for thermal management (air conditioning, heat exchangers, heat pipes, solar collectors, automotive cooling, radioactive waste cooling, and geothermal reservoirs), industrial processes (oil well drilling, chemical separation, and lubrication), structural engineering (steel bridge cables and rotary shafts), and environmental science (contaminant dispersion in soil).

As far as we know, a limited number of researches have been done to understand how changing the ratio of the nanoporous medium (porous media saturated with nanofluid) to nanofluid affects heat transmission by mixed convection inside an enclosure with a corrugated surface that houses a revolving cylinder. Thus, investigating the connection between the porous structure and the nanofluid behavior on a mixed convection heat transfer within a sinusoidal corrugated enclosure containing a revolving cylinder, both clockwise and counterclockwise, constitutes the primary innovation of this work. rotates in a clockwise and counterclockwise direction. The key parameters considered in this study are Lc =10^{-1} m, r = 1.5 ×10^{-2} m, ϕ=0.02, Da=10^{-3}, Ra=10^{4}, k_p= 0.845 m^2, Pr=6.2, amp=0.04 , N=6.

MATERIALS AND METHODS

Geometry

The current study geometry is depicted in Fig.(1). It consists of a square enclosure (L_C×L_C) with non-slip walls. The upper wall is insulated, while the vertical walls are at cold temperature (T_c), and the wavy bottom surface is at hot temperature (T_h). A solid, insulated cylinder with a radius (r) is located at the center of the enclosure. This cylinder can be rotated in either the clockwise (CW) or counterclockwise (CCW) direction at specific angular velocities.

Five scenarios have been considered based on the volume of nanoporous media (porous media filled with Al_2O_3 nanofluid) to the total volume (filled with nanaofluid) of the enclosure. The rest volume of the enclosure has been filled with Al_2O_3-water nanofluids (see Fig. 2).

MATHEMATICAL MODEL

Assumptions

The governor equations used in the current numerical analysis are based on the following assumptions (Al-kaby et al., 2023):

- The flow of fluid is assumed to be a two-dimensional, laminar and in steady state conditions.
- Due to high dilution, The nanofluid is taken as incompressible, single phase, and Newtonian.
- The nanoparticles are of the same size and shape and the porous medium is isotropic and homogeneous.
- All thermophysical features, except density, are assumed constant. The change in density creates the vertical component term that represents the momentum's body force in formula.
- There is a thermal equilibrium between the nanofluids inside the porous medium and the porous medium itself.
- The radiation effect is neglected.

Velocities and Temperature Modeling

Based on previous assumptions, the two dimensional governing equations for mass conservation, momentum, and energy can be written as (Kumar and Subudhi, 2021):

$$\frac{\partial \acute{u}}{\partial x}+\frac{\partial \acute{v}}{\partial y}=0 \quad (1)$$

$$\rho_{nf}\left(\acute{u}\frac{\partial \acute{u}}{\partial x}+\acute{v}\frac{\partial \acute{u}}{\partial y}\right)=-C_1\frac{\partial p}{\partial x}+C_2\,\mu_{nf}\left(\frac{\partial^2 \acute{u}}{\partial x^2}+\frac{\partial^2 \acute{u}}{\partial y^2}\right)-C_3\mu_{nf}\frac{\acute{u}}{K} \quad (2)$$

$$\rho_{nf}\left(\acute{u}\frac{\partial \acute{v}}{\partial x}+v\frac{\partial \acute{v}}{\partial y}\right)=-C_1\frac{\partial p}{\partial y}+C_2\mu_{nf}\left(\frac{\partial^2 \acute{v}}{\partial x^2}+\frac{\partial^2 \acute{v}}{\partial y^2}\right)-C_3\mu_{nf}\,\frac{\acute{v}}{K}+C_1\,(\rho\,\beta)_{nf}\,g(T-T_c) \quad (3)$$

$$\left(\acute{u}\,\frac{\partial T}{\partial x}+v\,\frac{\partial T}{\partial y}\right)=C_0\left(\frac{\partial^2 T}{\partial x^2}+\frac{\partial^2 T}{\partial y^2}\right) \quad (4)$$

where, C_o, C_1, C_2, C_3 are constants as indicated below:

	C_0	C_1	C_2	C_3
nanoporous	α_e	ε^2	ε	ε^2
nanofluid	αn	1	1	0

For expressing the governor formulas in dimensionless forms, the following dimensionless parameters have been considered.

$$R=\frac{r}{L_c},\ \Omega=\omega\,\frac{L_c^2}{\alpha_f},\qquad X=\frac{x}{L_c},\qquad Y=\frac{y}{L_c},\qquad \acute{U}=\acute{u}\frac{L_c}{\alpha_f},\qquad \acute{V}=\acute{v}\frac{L_c}{\alpha_f},\ P=\frac{pL_c^2}{\rho_f\alpha_f^2},$$

$$\acute{\theta}=\frac{T-T_c}{T_h-T_c},\quad Ra=\frac{g\beta_f L_c^3(T_h-T_c)}{\nu_f\ \alpha_f},Pr=\frac{\nu_f}{\alpha_f},\quad Ri=\frac{Ra\,Pr}{\Omega^2\,R^4},\quad Re=\frac{\omega\ r\ L_c}{\nu_f},Da=\frac{K}{L_c^2}$$

The final forms of formulas (1,2,3and4) are:

$$\frac{\partial \acute{U}}{\partial X}+\frac{\partial \acute{V}}{\partial Y}=0 \quad (5)$$

$$\left(\acute{U}\frac{\partial \acute{U}}{\partial X}+\acute{V}\frac{\partial \acute{U}}{\partial Y}\right)=-C_1\frac{\rho_f}{\rho_{nf}}\frac{\partial P}{\partial X}+\ C_2\frac{\nu_{nf}}{\alpha_f}\left(\frac{\partial^2 \acute{U}}{\partial X^2}+\frac{\partial^2 \acute{U}}{\partial Y^2}\right)-C_3\frac{\nu_{nf}}{\alpha_f}\frac{\acute{U}}{Da} \quad (6)$$

$$\left(\acute{U}\frac{\partial \acute{V}}{\partial X}+\acute{V}\frac{\partial \acute{V}}{\partial Y}\right)=-C_1\frac{\rho_f}{\rho_{nf}}\frac{\partial P}{\partial Y}+C_2\frac{\nu_{nf}}{\alpha_f}\left(\frac{\partial^2 \acute{V}}{\partial X^2}+\frac{\partial^2 \acute{V}}{\partial Y^2}\right)-C_3\frac{\nu_{nf}}{\alpha_f}\frac{\acute{V}}{Da}+C_1\,\frac{(\rho\,\beta)_{nf}}{\rho_{nf}\beta}\,Ra\,Pr\,\acute{\theta} \quad (7)$$

$$\acute{U}\ \frac{\partial \acute{\theta}}{\partial X}+\acute{V}\ \frac{\partial \check{\theta}}{\partial Y}=C_0\frac{1}{\alpha_f}\left(\frac{\partial^2 \acute{\theta}}{\partial X^2}+\frac{\partial^2 \acute{\theta}}{\partial Y^2}\right) \quad (8)$$

The thermophysical features formulas are: (Abu-Nada and Oztop, 2009):

$$\alpha_{nf} = \frac{k_{nf}}{(\rho\ cp)_{nf}} \tag{9}$$

$$\rho_{nf} = (1-\phi)\rho_f + \emptyset\rho_p \tag{10}$$

$$(\rho\ cp)_{nf} = (1-\phi)(\rho\ cp)_f + \phi(\rho\ cp)_p \tag{11}$$

$$(\rho\ \beta)_{nf} = (1-\phi)(\rho\ \beta)_f + \phi(\rho\ \beta)_p \tag{12}$$

The nanofluid's dynamic viscosity ratio given by Brink (Brinkman, 1952)

$$\mu_{nf} = \frac{\mu_f}{(1-\emptyset)^{0.25}} \tag{13}$$

The thermal conductivity ratio of nanofluid which has a spherical nanoparticles shape is approximated by the Maxwell-Garnetss (MG) model (Roslan et al., 2012):

$$\frac{k_{nf}}{k_f} = \frac{k_p + 2k_f - 2\emptyset(k_f - k_p)}{k_p + 2k_f + \emptyset(k_f - k_p)} \tag{14}$$

Table1 is presenting the thermophysical properties features of base fluid and Al_2O_3 nanoparticles.

The porous media properties formulas are (Abdulsahib, 2020, Mahdi et al., 2015):

$$\varepsilon = \frac{V_{void}}{V_{Total}} = 1 - \frac{V_{solid}}{V_{Total}} \tag{15}$$

$$\varepsilon = 0.3454 + 11.6985\ (d_p) \tag{16}$$

Permeability can be represented by Blake-Kozeny's equation as follow:

$$K = \frac{d_p^2\ \varepsilon^3}{150(1-\varepsilon)^2} \tag{17}$$

the effective thermal conductivity is represented as:

$$k_{eff} = (1-\varepsilon)k_s + \varepsilon k_{nf} \tag{18}$$

Where:

k_s :is the thermal conductivity of the solid matrix of porous media.
k_{nf} :is the thermal conductivity of nanofluids.

The Effective diffusivity of the porous media can be written as follow:

$$\alpha_{\text{eff}} = \frac{k_{\text{eff}}}{(\rho\, cp)_{\text{nf}}} \tag{19}$$

The local Nusselt number along the hot temp bottom wall can be defined as:

$$Nu_L = \frac{h}{k_f} \int_0^{\Delta x} \sqrt{1 + (\frac{dy}{dx})^2}\ dx \tag{20}$$

The local Nusselt number can be express as a function of the tmeprature gardinet as:

$$Nu = \frac{\partial \acute{\theta}}{\partial n} \tag{21}$$

While, the integration of the local Nusslet number results the mean Nusselt number.

$$\overline{\text{Nu}} = \frac{\int \text{Nu}\, dn}{\int dn} \tag{22}$$

The heat can be described utilizing heatlines, which are mathematically defined by heatfunction gained from heat fluxes by conduction (diffusion heatfunction) $(-\frac{\partial \acute{\theta}}{\partial X} - \frac{\partial \acute{\theta}}{\partial Y})$ in addition to heat fluxes by convection (convection heatfunction) $(\acute{U}\acute{\theta}, \acute{V}\acute{\theta})$.
The heatfunctions $(\acute{\Pi})$ inside the cavity can be written as :

$$\frac{\partial \acute{\Pi}}{\partial Y} = \acute{U}\acute{\theta} - \frac{\alpha_{\text{nf,p}}}{\alpha_f}\frac{\partial \acute{\theta}}{\partial X} \quad , \quad -\frac{\partial \acute{\Pi}}{\partial X} = \acute{V}\acute{\theta} - \frac{\alpha_{\text{nf,p}}}{\alpha_f}\frac{\partial \acute{\theta}}{\partial Y}$$

The final heatfunction derives from subsutiution the above euations in the energy formula (Eq. 8) as follows:

$$\frac{\partial^2 \acute{\Pi}}{\partial X^2} + \frac{\partial^2 \acute{\Pi}}{\partial Y^2} = \frac{\partial}{\partial Y}(\acute{U}\acute{\theta}) - \frac{\partial}{\partial X}(\acute{V}\acute{\theta}) \tag{23}$$

The streamfunction (ψ) is used to describe fluid motion. The streamfunction formulas are gained from velocity components U and V as follow:

$$\acute{U} = \frac{\partial \psi}{\partial Y}, \qquad \acute{V} = -\frac{\partial \psi}{\partial X}$$

$$\frac{\partial^2 \psi}{\partial X^2} + \frac{\partial^2 \psi}{\partial Y^2} = \frac{\partial \acute{U}}{\partial Y} - \frac{\partial \acute{V}}{\partial X} \tag{24}$$

The entropy generation rate inside the enclosure is produced either by the flow of heat or the dissipating viscous. The form of local entropy generation rate can be desecribed as (Ingham et al., Vadász, 2008):

$$S_{gen} = S_{gen,T} + S_{gen,\mu} \quad (25)$$

$$S_{gen,T} = \frac{k_{nf}}{k_f}\left[\left(\frac{\partial \acute{\theta}}{\partial X}\right)^2 + \left(\frac{\partial \acute{\theta}}{\partial Y}\right)^2\right] \quad (26)$$

$$S_{gen,\mu} = \chi\left[2\left(\frac{\partial \acute{U}}{\partial X}\right)^2 + 2\left(\frac{\partial \acute{V}}{\partial Y}\right)^2 + \left(\frac{\partial \acute{U}}{\partial Y} + \frac{\partial \acute{V}}{\partial X}\right)^2\right] \quad (27)$$

Where $\chi = \frac{T_o\, \acute{U}_o^2}{\Delta T^2}\frac{\mu_{nf}}{k_f}$

The dimensionless entropy generation is

$$S_{gen} = s_{gen}\frac{T_o^2\, L_c^2}{k_f\, \Delta T^2}$$

The mean entropy generation in all calculations domains is determine by intergration the local entopy generation within the computational domain as follows:

$$\dot{S}_{gen} = \int S_{gen}\, dA \quad (28)$$

Bejan number (Be): is alternative value that can explain the distribution of irreversibility, which represents the relative contribution of heat transfer irreversibility (caused by temp variances) compared to viscous dissipation irreversibility (caused by friction) within a system, it is defined as:

$$B_e = \frac{\dot{S}_{gen,T}}{\dot{S}_{gen}} \quad (29)$$

Where, $Be_{av} > 0$ means dominating of heat transfer irreversibility, and $Be_{av} < 0.5$ means dominating of fluid friction irreversibility (Basak et al., 2012).

Boundary Conditions

In this paper, the boundary conditions are:

At $X = 0$ and 1, $\quad 0 \le Y \le 1, \quad \acute{U}_{nf,p} = \acute{V}_{nf,p} = 0\ , \acute{\theta}_{nf,p} = 0$

At $Y = 1, \quad 0 \le X \le 1\ , \quad \acute{U}_{nf,p} = \acute{V}_{nf,p} = 0\ , \frac{\partial \acute{\theta}_{nf,p}}{\partial X} = 0$

At corrugated bottom wall

For $Y = 0.04\, Sin(\pm 2N\pi X)\ , \quad 0 \le X \le 1\ , \quad \acute{U}_{nf,p} = \acute{V}_{nf,p} = 0\ , \acute{\theta}_{nf,p} = 1$

On the insulated solid surface of the rotating circular cylinder:

$X = 0.5 + R\,Cos(\pm 2\pi t), Y = 0.5 + R\,Sin(\pm 2\pi t), \qquad t = 0 \text{ to } 1$

$$\acute{U}_{nf,p} = \acute{U}o\frac{(Y - Yo)}{R} = \Omega(Y - Yo)$$

$$\acute{V}_{nf,p} = \acute{U}o\frac{(X - Xo)}{R} = \Omega(X - Xo)$$

$$\frac{\partial \acute{\theta}_{nf,p}}{\partial nn} = 0 \quad , \qquad \frac{\partial \acute{\theta}_{P}}{\partial nn} = 0$$

At the space between nanofluid-porous media:

$$\frac{\partial \acute{\theta}_{nf}}{\partial y} = \frac{k_{eff}}{k_f}\frac{\partial \acute{\theta}_{p}}{\partial y} \qquad , \acute{\theta}_{nf} = \acute{\theta}_{p}$$

$$\acute{U}_{nf} = \acute{U}_{P}\,, \acute{V}n_f = \acute{V}_{P}\,,$$

Where:

$\frac{\partial \acute{\theta}_{nf}}{\partial nn}$ and $\frac{\partial \acute{\theta}_{P}}{\partial nn}$: are for the nanofluid layer and the porous layer, respectively.

Xo and Yo : are the cylinder positions inside the cavity.

nn : is a vector perpendicular to the cylinder.

The boundary conditions for streamfunction are:

$Y = 0$ and 1 bottom and top wall $0 \le X \le 1, \qquad \psi = 0$

$X = 0$ and 1 Left and right wall $0 \le Y \le 1, \qquad \psi = 0$

Cylinder $X = 0.5 + R\,\cos in(\pm 2\pi t)$, $Y = 0.5 + R\,Sin(\pm 2\pi t)$, $t = 0$ to 1,

$$\frac{\partial \psi}{\partial Y} = \acute{U}_0 = \Omega(Y - Y_0), \qquad \frac{\partial \psi}{\partial X} = -\acute{V}_0 = \Omega(X - X_0)$$

In addition, the heatfunction's boundary conditions can be described as:

$At\ X = 0, Y = 1, \qquad \acute{I}(0,1) = 0$

$$At\ X = 0, Y = 0, \qquad \acute{I}(0,0) = \acute{I}(0\,,1) - \int_0^1 \frac{\partial\, \acute{I}}{\partial\, Y}\, dY$$

$$\acute{I}(0\,,0) = \acute{I}\,(0\,,1) + \int_0^1 \frac{\alpha_{nf,p}}{\alpha_f}\frac{\partial \acute{\theta}}{\partial X} dY$$

$At\ X = 1, Y = 1, \qquad \acute{I}(1,1) = 0$

$$At\ X = 1, Y = 0, \qquad \acute{I}(1,0) = \acute{I}(1\,,1) - \int_0^1 \frac{\partial\, \acute{I}}{\partial\, Y}\, dY$$

$$\acute{\Pi}(1,0) = \acute{\Pi}(1,1) + \int_0^1 \frac{\alpha_{nf,p}}{\alpha_f} \frac{\partial \acute{\theta}}{\partial X} dY$$

NUMERICAL SOLUTION AND THE VALIDATION

Numerical Simulation

The Finite Elements Method based on the variational formulation is used to obtained the solution of the dimensionless governing formulas (Eqs. 5-29). In the current work, the steady-state velocity, temperature, and pressure distributions were calculated using a finite element approach, incorporating non-uniform triangular elements with mesh refinement in areas of high gradients and geometric complexity. The weak formulation of the governing equations was derived using the Galerkin method, followed by standard assembly of element equations, the imposition of boundary conditions, and solution of the resulting system utilizing an improved algorithm developed by the Rannacher method via an in-house developed C++ code (Al-Zamily, 2016). The program's procedural flowchart is illustrated in Fig. (3).

In the present study, the convergence criterion for streamfunction and isotherms are:

$$\frac{\sum_{i=1}^{N} \left| \psi_i^{m+1} - \psi_i^{m} \right|}{\sum_{i=1}^{N} \left| \psi_i^{m+1} \right|} \leq 10^{-7} \quad \text{and} \quad \frac{\sum_{i=1}^{N} \left| \acute{\theta}_i^{m+1} - \acute{\theta}_i^{m} \right|}{\sum_{i=1}^{N} \left| \acute{\theta}_i^{m+1} \right|} \leq 10^{-7}$$

A grid accuracy test has been carried out to conduct the solution grid independently. To make sure that the solutions of the numerical results are not depend of the grid, accuracy testing is required. A series of trial calculations were performed for various grids and element numbers to confirm the grid solution independently utilizing several non-uniform grid systems in the instance as shown in Table 2. Findings of those trials are displayed in Table 2 for ϕ =0.02, Ra=10^4, Da=10^{-3}, r = 1.5 $\times 10^{-2}$ m, L_c =10^{-1} m, and Pr=6.2. Based on Table 2, the results for 50 grid and 60 grid demonstrate very little variances, therefore, a 50 grid findings are acceptable to save a computational time (see Fig. 4).

Validation

To check the accuracy of the current results, the isothermes and streamlines are compared with Selimefendigil et al. [10] at Darcy numbers, Da = 10^{-2}, 10^{-3}, and 10^{-5}, as indicted by Fig. 5. The comparison revealed a good agreement between the two works.

RESULTS AND DISCUSSION

The effect of varying nanoporous media volume to the total cavity volume (HH =0%, 25%, 50%, 70%, and 100%) on the heatlines, isotherms, streamfunction, dimensionless entropy, velocity vectors (U, V), Bejan number, and Nusselt numbers are cosidered. The analysis covered a range of cylinder angular velocities (Ω=0, ±3000, ±6000):

Heatlines

Heatlines are used to describe the heat flow through the enclosure from the hot source (corrugated bottom wall) to the cold sources (vertical walls). Counterclockwise heat flow is represented by a positive heat function, and clockwise heat flow is represented by a negative heat function. Heatlines for different values of the nanoporous media to cavity volume ratio at different angular velocities are plotted in Fig.(6).

At Ω=0, conduction is the main method to transfer heat and govern the heat flow within the cavity, demonstrated by a straight heatline. Due to symmetrical boundary conditions along the Y-axis, the heat is distributed equally to each cold wall. Because heat tends to travel a shorter distance due to low thermal resistance, the bulk of heatlines (about 60%) are found near the corners between the hot and cold surfaces. When the cylinder has an angular velocity, convection takes over as the main way of influencing the heatline magnitudes, allowing them to follow the velocity vector in the direction of the cold surface. Typically, the circulation form of heatlines is caused by the convection effect, which is reduced as the porous media volume ratio rises. Hence, the heatline magnitudes increase as the conduction effect rises. A more straight path has appeared across the porous media region as the porous media volume ratio is increased. Heatlines maintain their maximum absolute magnitude even when their orientation is changed from clockwise to counterclockwise. A rise in Ω will intensify the heatline's size because of the increase convection effect. At Ω=0, The heat flux is split equally between the vertical cold walls.

When Ω=+3000, forced convection causes 55% of the total heat flow to travel a longer journey around the cylinder and the other part to travel a shorter path towards the vertical cold right side wall. while, for Ω=+6000, about 20% of the heat flux traveling in the direction of the vertical cold right side wall travels a shorter path, while the remaining 80% travels around the cylinder over a longer one. Increasing HH will increase the percentage of heat through the short path due to the reduction of fluid movement at lower areas. The heatlines magnitude rises as HH rises from 0 to 0.25 at Ω=0 and Ω≠0. In general, increasing HH above 0.5 will not affect the heatlines magnitude since increasing nanoporous media volume generally leads to a reduction in convection heat transfer and the majority of heat will transfer to the cold lower walls.

Isotherms

In Fig.(7), the infeluence of the dimensionless cylinder angular velocity and the ratio of nanoporous media volume to cavity volume on the isotherms are sketched. These isotherms are perpendicular to the heat flux (heatlines), especially at Ω=0. At Ω=0, the isotherms perpendicularly depart from the corrugated hot surface towards the insulated walls. Since most of the heat moves from the wavy hot wall to the lower side of the vertical walls, the denser isotherms are located next to the hot wall. The isotherms are symmetrically positioned around the vertical midline of the enclosure, indicating uniform heat transfer. Heatlines move in the direction of the corrugated hot wall as the conduction at the lower parts of the cold walls increases. for Ω≠0 and counter-clockwise rotation, the isotherms trend towards the right wall since forced convection is enhanced and most of the heat moves to the right cold wall. When the cylinder rotates in a clockwise orientation, similar behavior is seen, with the isotherms shifting in the direction to the left wall. As HH magnitude increases, isotherms tend to become flatter due to enhanced conduction. which leads to lower particle velocities within the porous media.

Streamfunction:

The streamfunction is plotted for several values of HH and Ω in Fig. (8). At Ω=0, the buoyancy force produces two symmetrical vortices with different directions, which manage the flow contours in the enclosure. When the nanoporous media volume ratio (HH) increases, the range of streamfunction is reduced. The absolute magnitude of streamfunction drops to 0.05-0.33 at HH=0.25% and keeps dropping more to 0-0.11 at HH=1. Overall, the range of absolute magnitude of stramfunction decreases as the nanoporous media volume ratio (HH) increases. When Ω≠0, the maximum absolute stream function rises with increasing velocity and decreases with increasing HH. The influence of Ω on the streamfunction is getting less as the HH value increases. At Ω=0, as the HH grows from 0 to 0.25, the maximum streamfunction magnitude drops. Maximum magnitudes won't be noticeably affected by the increase in HH of more than 0.5 because the majority of heat is carried through the cold walls' lower side potion. Since the rotating cylinder is completely covered with nanoporous media at/and above 0.75, the max streamfunction magnitude drops when Ω≠0 as HH grows up to that point. Table 3 shows the maximum streamfunction magnitudes with changing HH at different angular velocities.

Dimensionless Entropy

The dimensionless entropy inside the cavity is shown in Fig. (9) for different cylinder-rotating angular velocities and volume ratios of nanoporous media. At Ω=0, the dimensionless entropy is organized symmetrically around the vertical center line of the cavity and its magnitude drops with an increase in HH. The lowest magnitudes of the dimensionless entropy are found near the insulated top wall because of low heat transfer and poor fluid circulation. Whereas, the highest magnitudes are found near the highest heat transfer area at the corners of the bottom hot wavy surface (close to the junction between hot and cold surfaces).

The dimensionless entropy generation lines in Fig. (9) are clearly aligned with the heatlines, indicating that conduction serves as the main governing factor in the system, particularly at high HH. At Ω=±3000, forced convection begins to dominate the flow and causes an increase in dimensionless entropy magnitude by up to 71 times relative to Ω=0. The maximum magnitudes of the dimensionless entropy are found near the revolving cylinder and get smaller as they move away from it. This is because the entropy resulting from heat movement is lower than the entropy resulting from viscous dissipation. Comparing Ω=±3000 to Ω=±6000, the dimensionless entropy magnitude grew by approximately 5 times. The dimensionless entropy can be decreased by up to (1/143) (HH=1 magnitude/HH=0 magnitude) by increasing the HH. This result is due to the viscosity impact that reduces the entropy generation.

Bejan Number

Fig.(10) illustrates the variation of Bejan number (Be) with various Ω and HH. Because of the symmetrical boundary conditions at the two vertical walls, Be is symmetrically distributed around the Y-centerline of the cavity at Ω=0. For Ω=0 and HH=0, the influence of temperature and buoyancy force results in the emergence of a multiple (Be) vortex. The maximum Be number is related to the smaller velocity gradient. The impact of buoyancy force is reduced as (HH) magnitudes rise, and the Be magnitudes keep growing until reach the maximum values at HH=1. The maximum Be can appear close to the vortices surrounding the revolving cylinder at different angular velocities (clockwise or counterclockwise). As the nanoporous media ratio (HH) increases, friction force and (Be) increase, especially far away from the circular cylinder, Ultimately, high Be fills all the enclosure except the area surrounding the circular cylinder.

Velocity Vector

Fig. (11) shows the contour lines of the velocity vector (U˘,V˘) at different HH magnitudes and angular velocities (Ω=0, ±3000, ±6000). At Ω=0, the buoyancy force governs the heat and flow patterns inside the enclosure (free convection). Due to temperature variations at the hot wavy base wall and the maximum heat transfer to the bottom corners of the vertical cold walls, large circulations show up close to the hot base wall. With symmetrical boundary conditions, the velocity vector took a symmetrical pattern around the vertical center line of the cavity. Finally, with the increase of HH, the absolute maximum velocity vector decreases. Table 4 shows the percentage reduction in the maximum velocity vector with increasing HH.

The maximum velocity vector will decrease by 75.5% when HH is increased from 0 to 0.25. Whereas, the maximum velocity vector will be reduced by 41.35% at HH of 0.5 compared to HH=0.25. Because the porous media layers enhance the quantity of heat rate to the cold walls, further increase in HH will not significantly affect the maximum velocity vector.

The effect of Ω is noticeable for small HH. The flow starts to be dominated by forced convection and the velocity vector values near the revolving cylinder increase as Ω rises. The maximum absolute velocity vector magnitude is independent of rotational direction. With increasing porous medium (HH) volume ratio, the effect of the angular velocity decreases.

At HH=0.5, an interesting behavior for velocity vectors can be observed, the velocity vector for the nanofluid layers first decreases as they travel away from the solid cylinder and then increases and decreases. When the layer is changed with dense fluid, the reaction of the velocity direction shifts which causes this behavior. At $\Omega \neq 0$, the maximum velocity vector always relates to the cylinder's rotational velocity.

Nusselt Number

In Fig.(12), the mean value of Nusselt number ($\overline{Nu}$) along the Sinusoidal bottom wall for all cases at various values of HH and Ω is shown. As the rotational velocity increases, the mean Nusselt number rises until it reaches a plateau, where its value slightly varies. This behavior indicates the transition from free convection (at $\Omega=0$) to mixed convection as rotational velocity increases. Further increasing the rotation speed ($\Omega>\pm6000$) does not effectively improve ($\overline{Nu}$), suggesting that further increase does not significantly enhance heat transfer due to increased viscous dissipation. At HH=0, $\overline{Nu}$ has the highest value compared with the other cases. As the nanoporous media level increases (HH>0), the resistance to fluid flow offered by the porous medium increases, which hinders convective heat transfer.

CONCLUSIONS

A square cavity with a sinusoidal wavy bottom wall and insolated rotating cylinder at 0, ±3000, and ±6000 is investigated in this work to determine the effect of the nanofluid/nanoporous media volume ratio on the mixed convection heat transfer. The main constrain parameters that taken into account are Pr=6.2, $r = 1.5 \times 10^{-2}$ m, $Lc = 10^{-1}$ m, ϕ=0.02, $Ra=10^4$, $Da=10^{-3}$, k_p= 0.845, amp=0.04, and N=6. The following conclusion draws from this study.

1- The isotherms symmetrically depart from the corrugated hot surface towards the insulated walls and den close to the hot wall. As HH increases, they become flatter due to a decrease in particle velocity.
2- The maximum velocity vector decreases by 75.5% when HH increases from 0 to 0.25. At HH = 0.5 It is decreased by 41.35% comparing to 0.25 and further increase in HH will not significantly effect the maximum velocity vector.
3- At $\Omega=0$, the bulk of heatlines (about 60%) are found near the corners between the hot and cold surfaces. As the nanofluid/nanoporous media volume ratio rises, the values of heatline increase due to rise in conduction and the path of heatlines across the porous media region becomes more forward. At both cases of $\Omega=0$ and $\Omega\neq0$ the heatline values increase as HH increase from 0 to 0.5 while these values won't be significantly affected by an increase of HH more than 0.5.
4- When Ω is increased to ±6000, the dimensionless entropy increased by about 5 times compared to $\Omega=\pm3000$. Increasing the HH will reduce the dimensionless entropy by up to (1/143).
5- When Ω increases, the forced convection component becomes more dominant, leading to an increase in the mean Nusselt number until reaches a plateau.

FIGURES AND TABLES

Figures

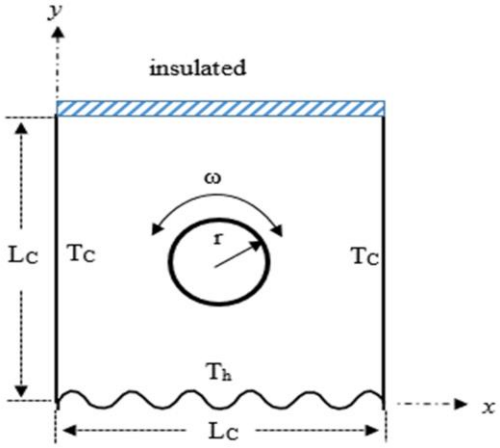

Fig.(1): Schematic diagram of physical problem.

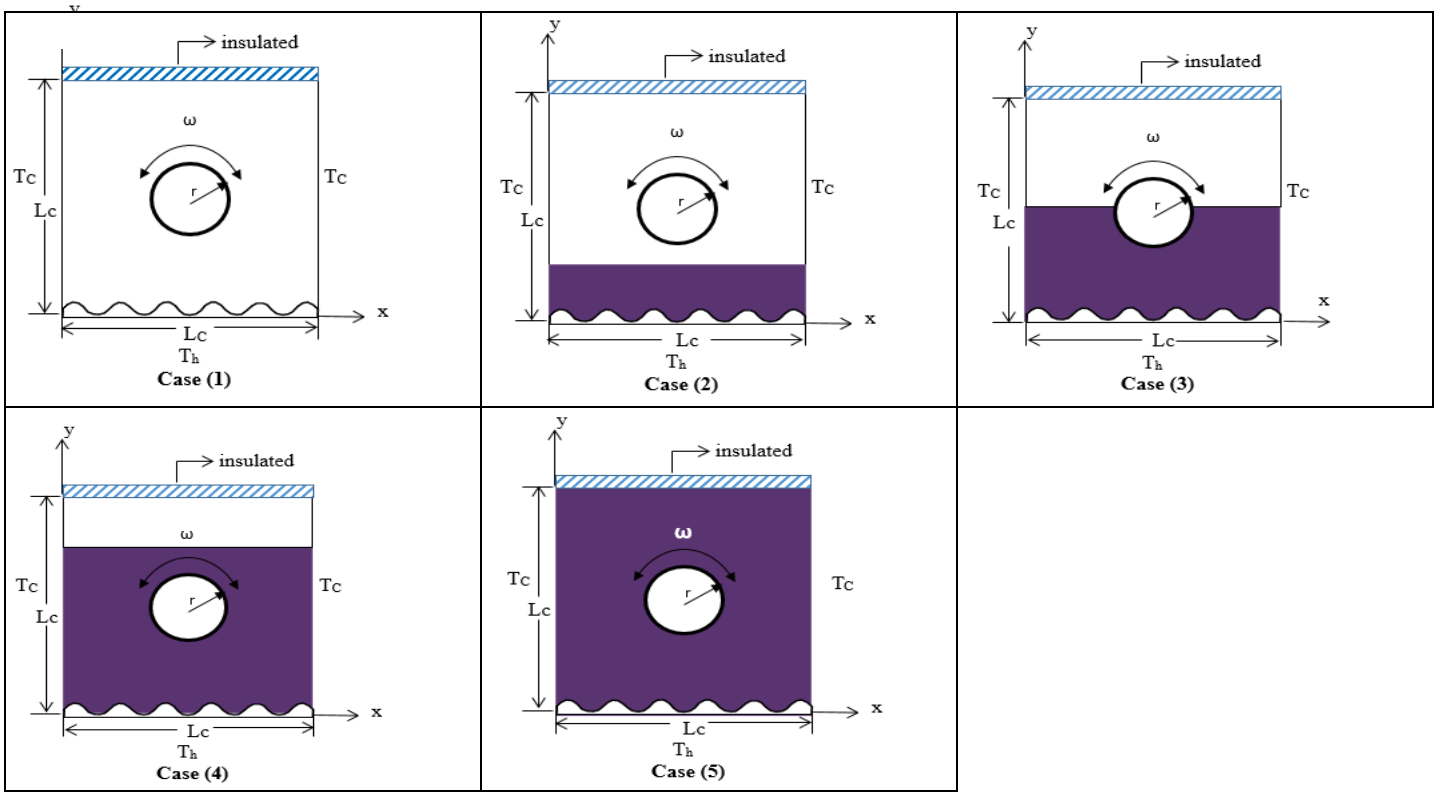

Fig. (2): Schematic of the studied cases: light area represents the Al_2O_3/water nanofluid and dark area represents the nanoporous media (porous media saturated with Al_2O_3/water nanofluid).

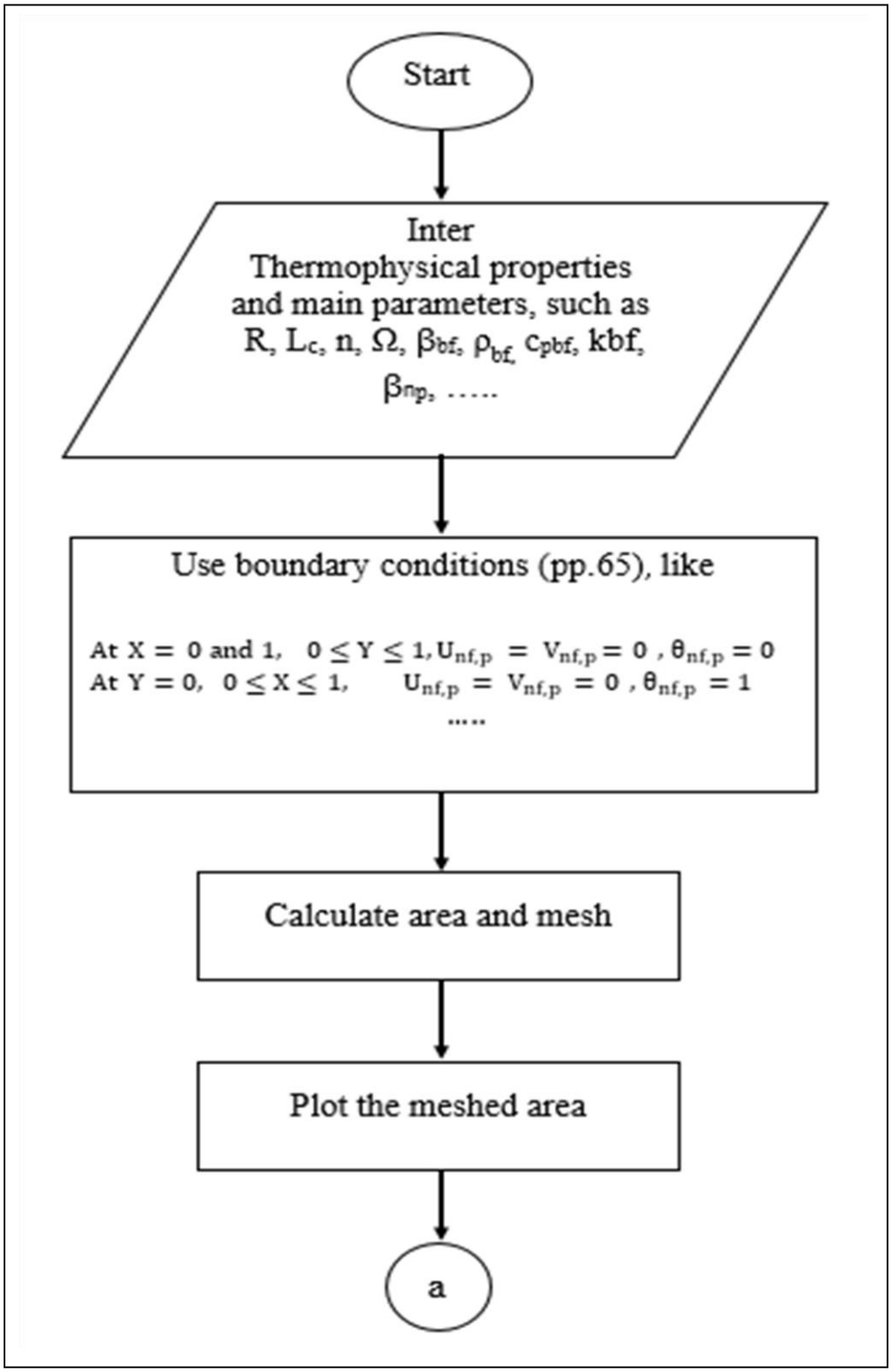
Start
Inter
Thermophysical properties
and main parameters, such as
R, L_c, n, Ω, β_{bf}, ρ_{bf}, c_{pbf}, kbf,
β_{np}, ...
Use boundary conditions (pp.65), like
At X = 0 and 1, $0 \leq Y \leq 1, U_{nf,p} = V_{nf,p} = 0$, $\theta_{nf,p} = 0$
At Y = 0, $0 \leq X \leq 1$, $U_{nf,p} = V_{nf,p} = 0$, $\theta_{nf,p} = 1$
.....
Calculate area and mesh
Plot the meshed area
a

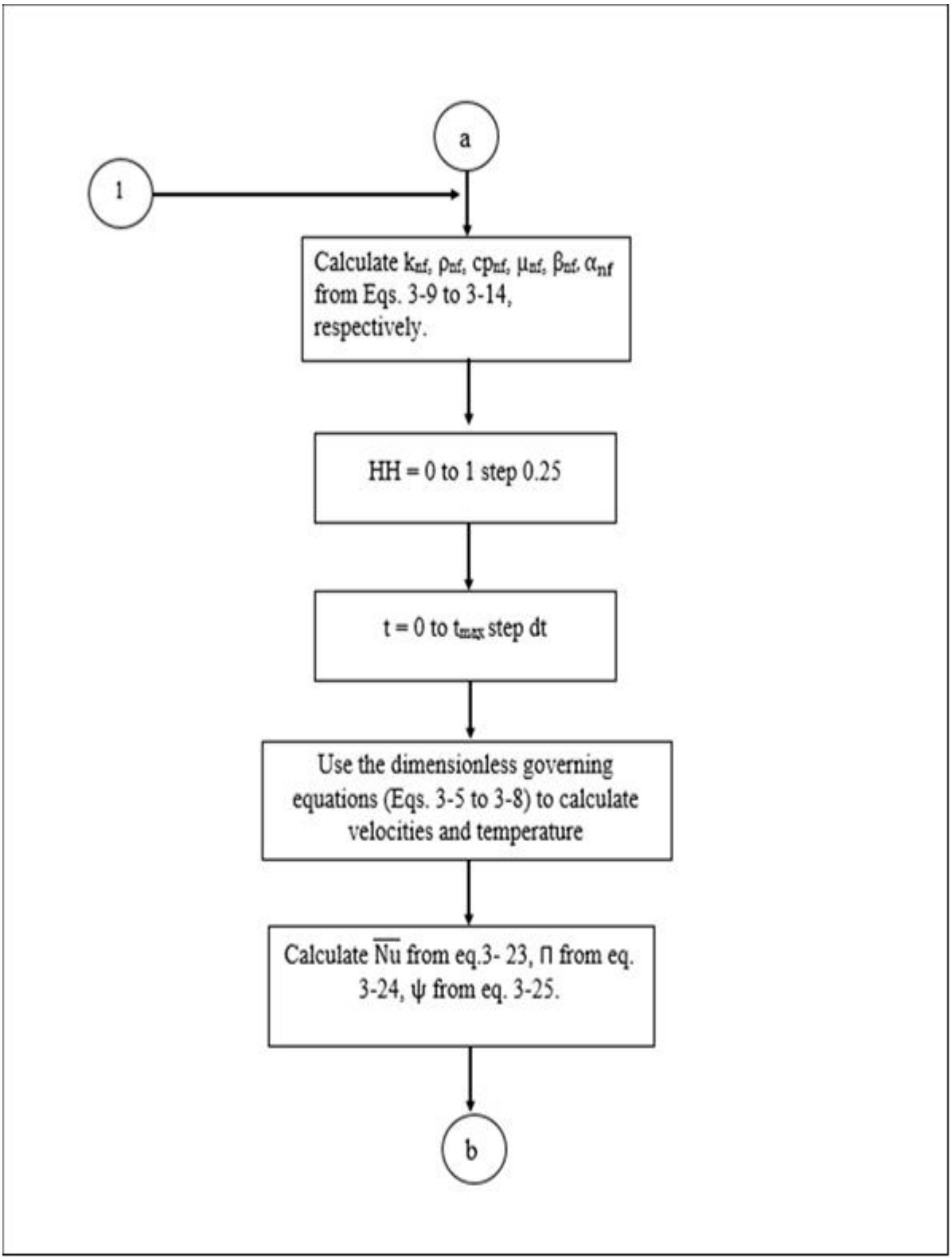
a
1
Calculate k_{nf}, ρ_{nf}, cp_{nf}, μ_{nf}, β_{nf}, α_{nf} from Eqs. 3-9 to 3-14, respectively.
HH = 0 to 1 step 0.25
t = 0 to t_{max} step dt
Use the dimensionless governing equations (Eqs. 3-5 to 3-8) to calculate velocities and temperature
Calculate $\overline{Nu}$ from eq.3- 23, Π from eq. 3-24, ψ from eq. 3-25.
b

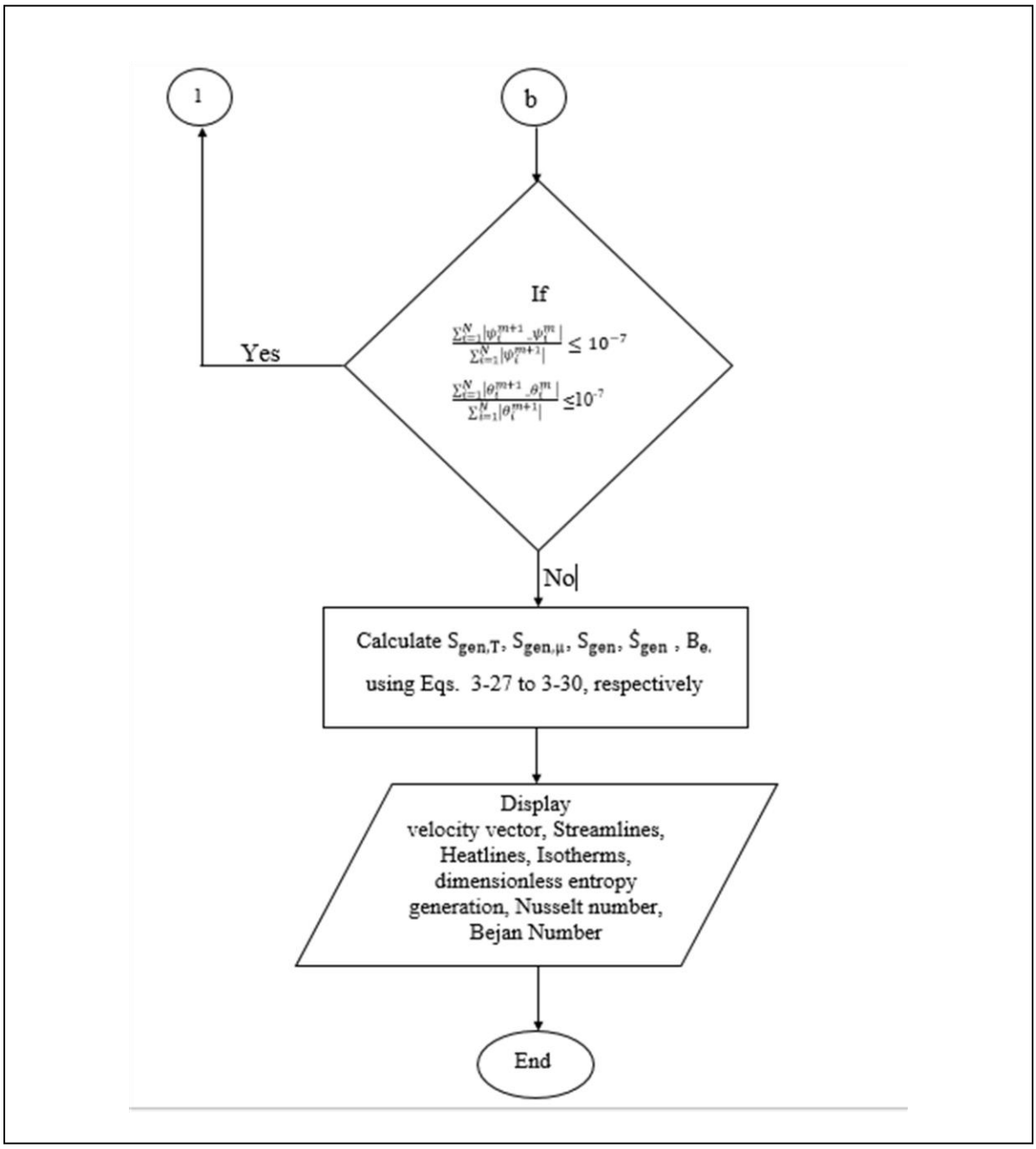

Fig. (3): Schematic Flow Chart of program.

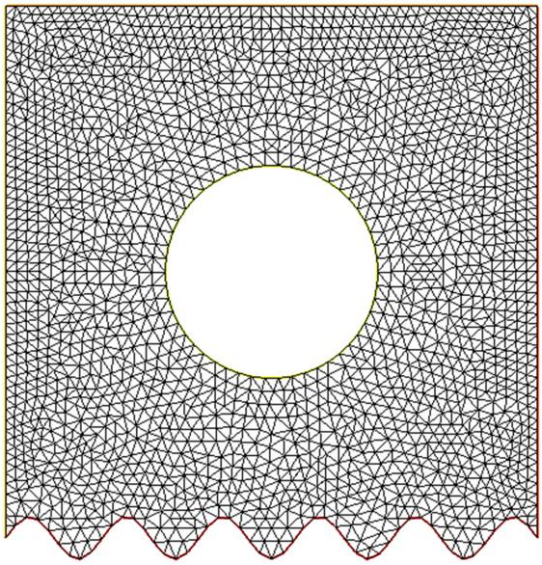

Fig. (4): The mesh of the computational space.

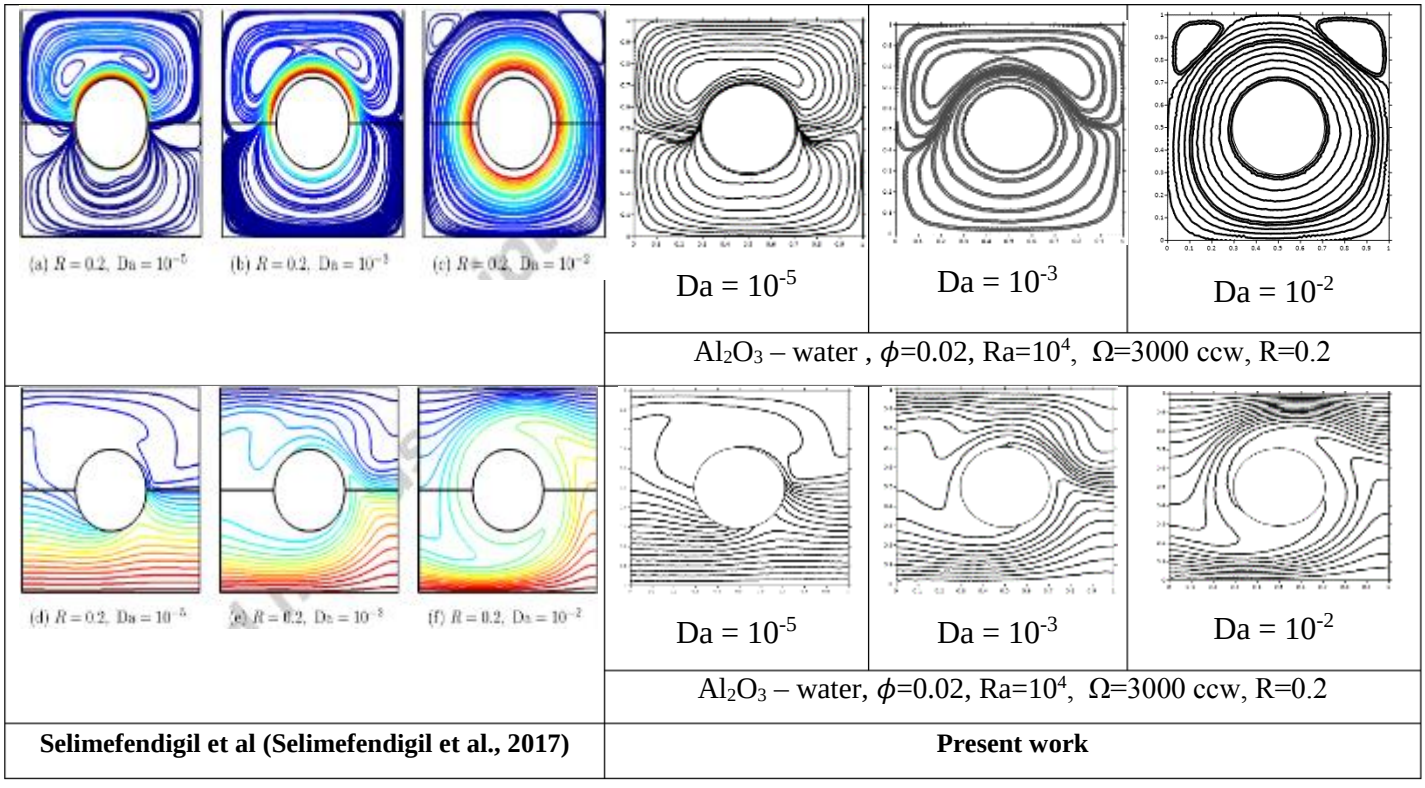

Fig. (5): A comparison of isotherm and streamlines between current work Selimefendigil et al (Selimefendigil et al., 2017) with mixed convection in a square cavity for Da = 10^{-2}, 10^{-3}, and 10^{-5}.

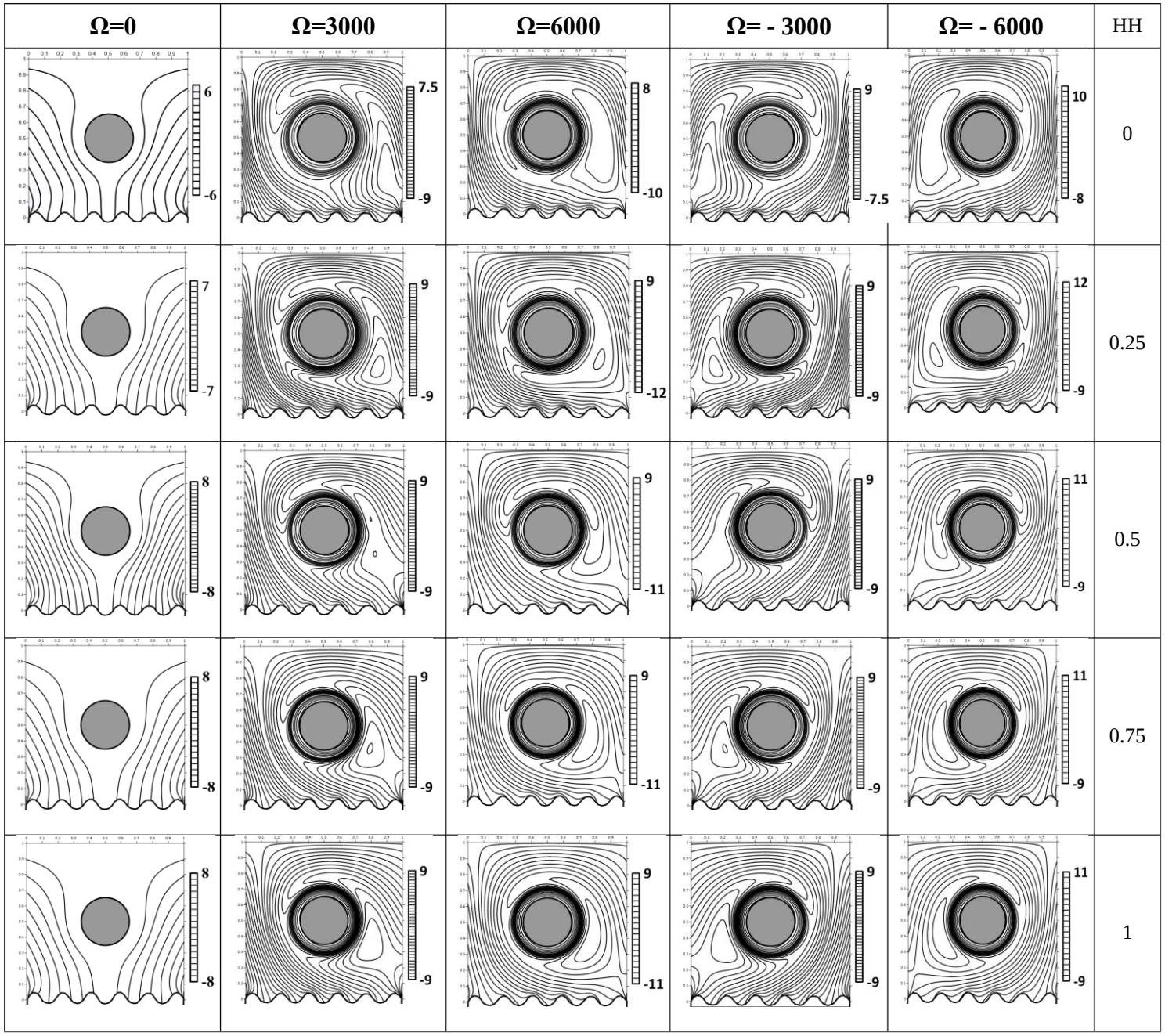

Fig. (6): Heatlines of Al_2O_3-water nanofluid at various dimensionless cylinder angular velocities (Ω=0, ±3000, ±6000) and various magnitudes of HH= (0,0.25,0.5,1) with ϕ=0.02, Ra = 10^4, Da = 10^{-4} and R=0.15.

Fig. (7): Isotherms contours of Al_2O_3-water nanofluid at various dimensionless cylinder angular velocities (Ω=0, ±3000, ±6000) and various magnitudes of HH= (0,0.25,0.5,1) with ϕ=0.02, Ra = 10^4, Da = 10^{-4} and R=0.15.

Ω=0	Ω=3000	Ω=6000	Ω= - 3000	Ω= - 6000	HH
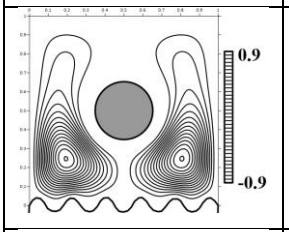	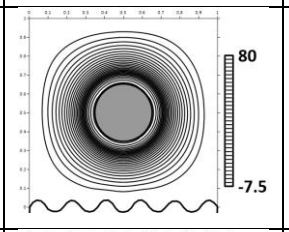	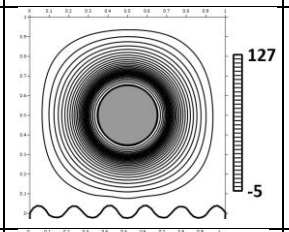	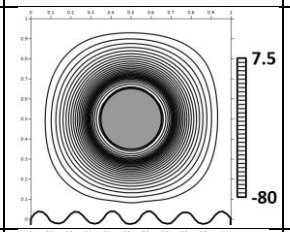	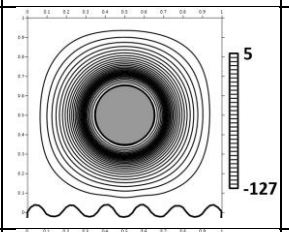	0
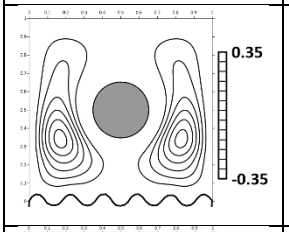	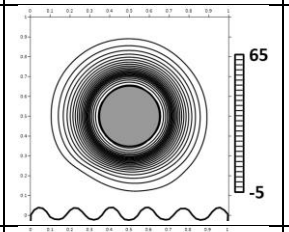	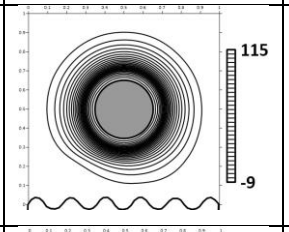	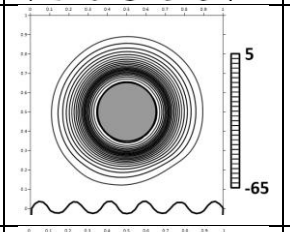	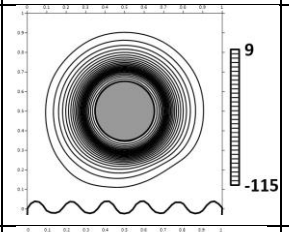	0.25
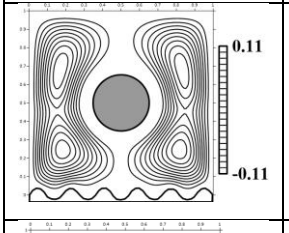	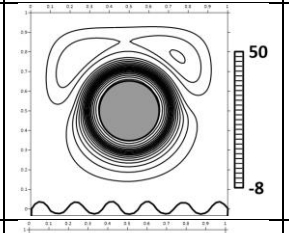	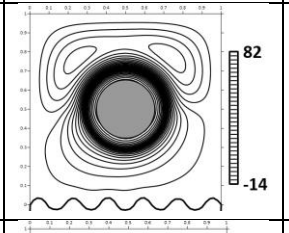	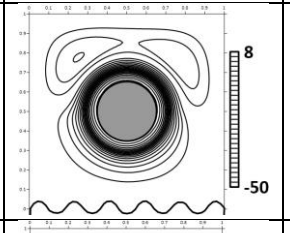	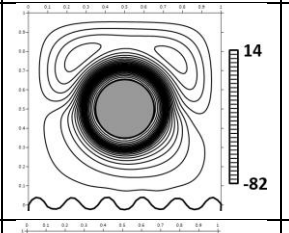	0.5
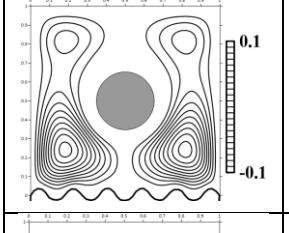	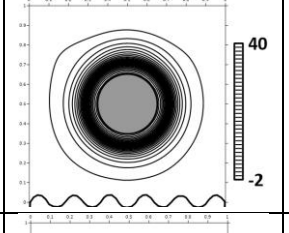	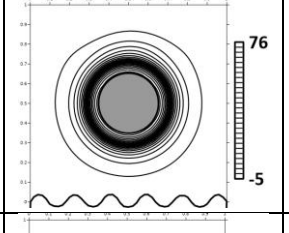	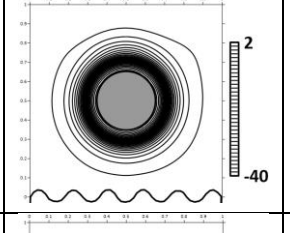	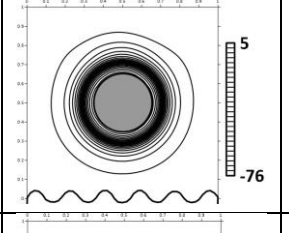	0.75
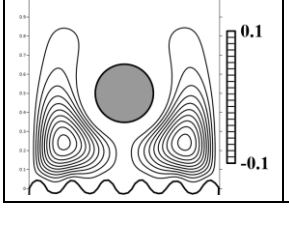	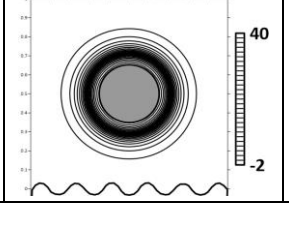	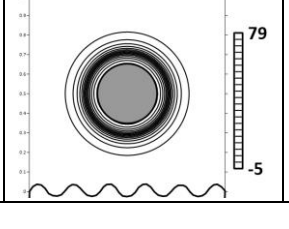	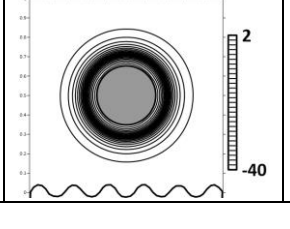	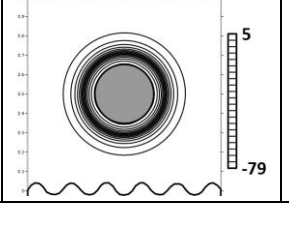	1

Fig. (8): Streamlines contours of Al_2O_3 – water nanofluid at various dimensionless cylinder angular velocities (Ω=0, ±3000, ±6000) and various magnitudes of HH= (0,0.25,0.5,1) and ϕ=0.02, Ra = 10^4, Da = 10^{-4} andR=0.15.

Ω=0	Ω=3000	Ω=6000	Ω= - 3000	Ω= - 6000	HH
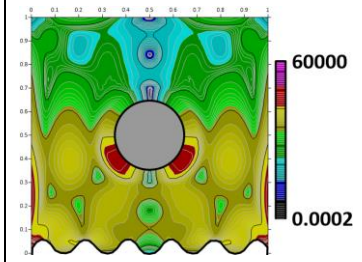	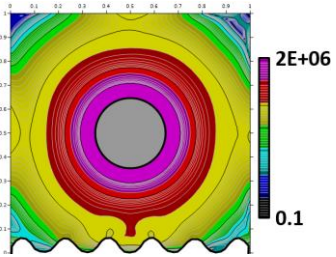	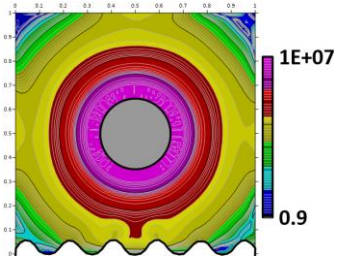	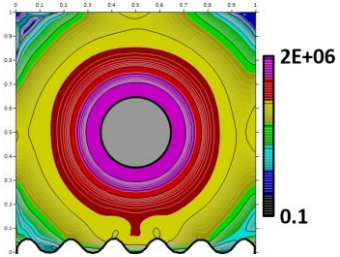	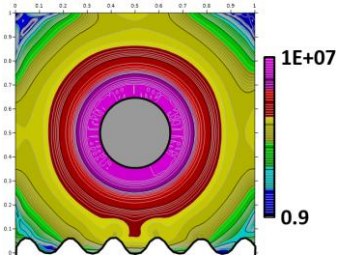	0
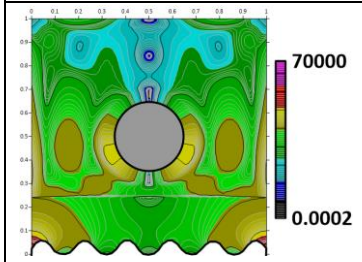	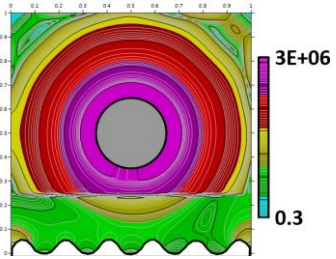	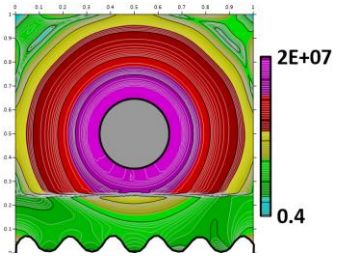	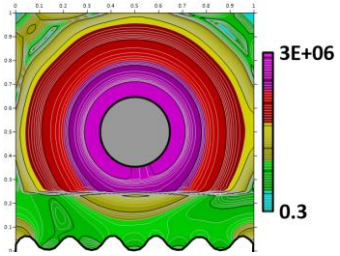	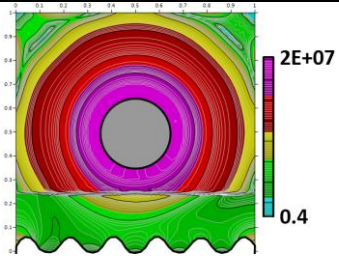	0.25
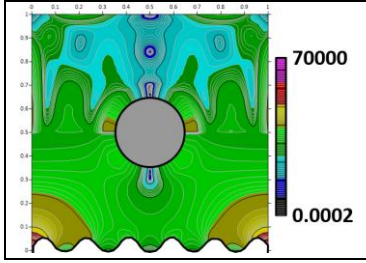	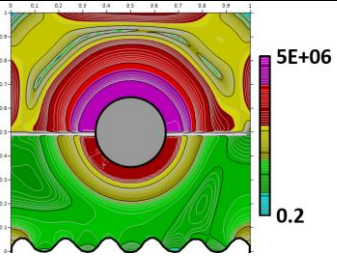	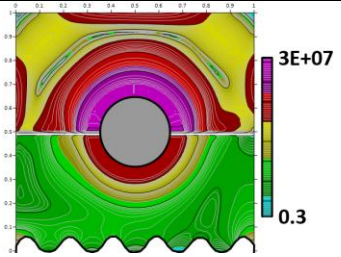	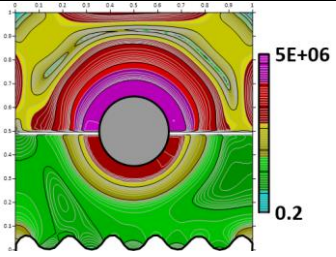	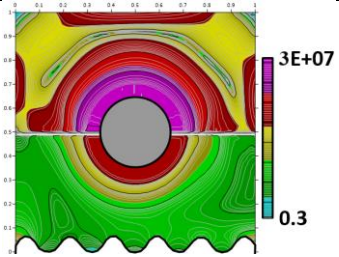	0.5

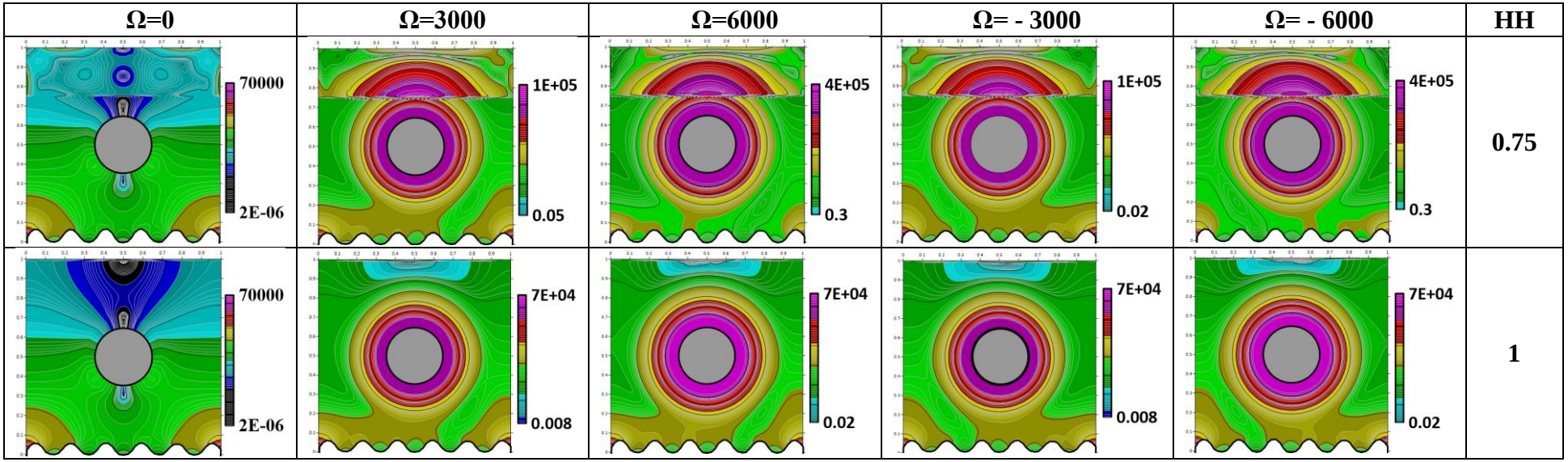

Fig. (9): Dimensionless Entropy contours of Al_2o_3 – water nanofluid at various dimensionless cylinder angular velocities (Ω=0, ±3000, ±6000) and various level of HH= (0,0.25,0.5,1) from the cavity height and ϕ=0.02%, Ra = 10^4, Da = 10^{-4} and R=0.15.

Ω=0	Ω=3000	Ω=6000	Ω= - 3000	Ω= - 6000	HH
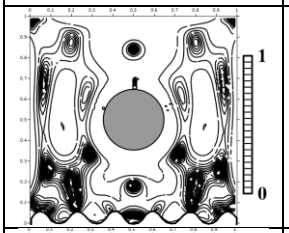	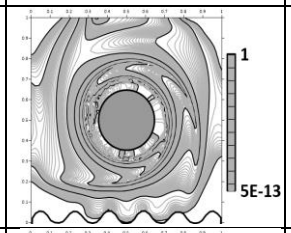	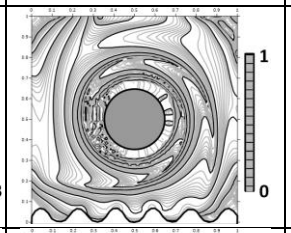	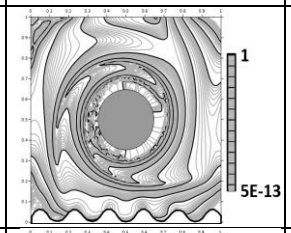	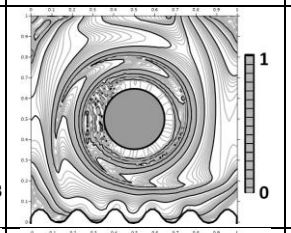	0
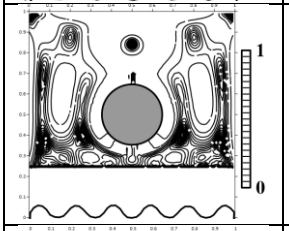	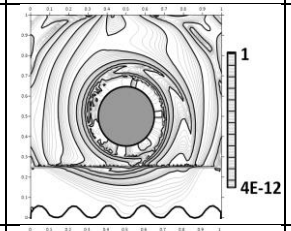	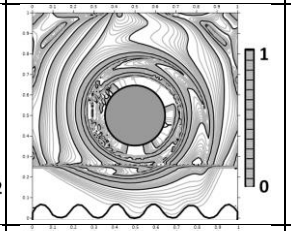	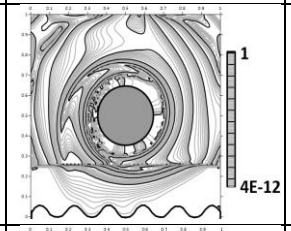	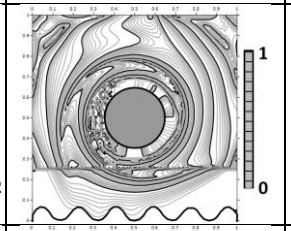	0.25
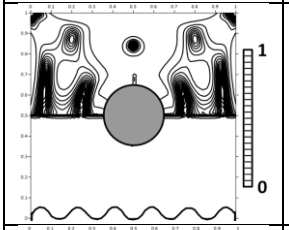	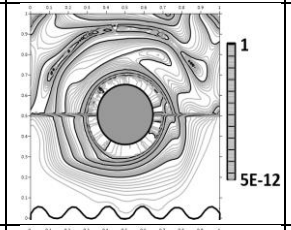	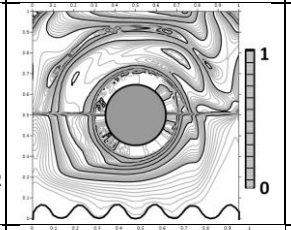	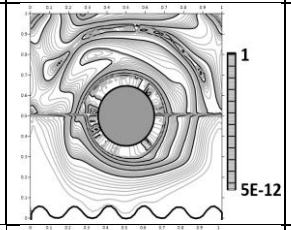	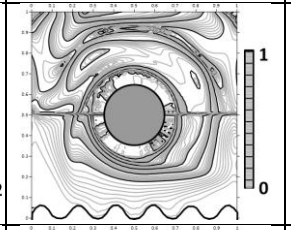	0.5
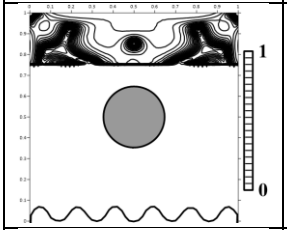	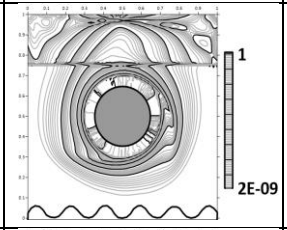	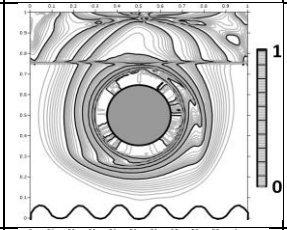	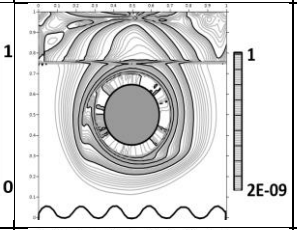	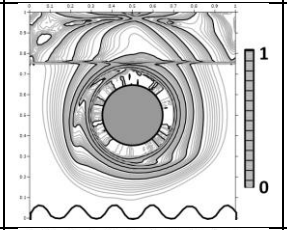	0.75
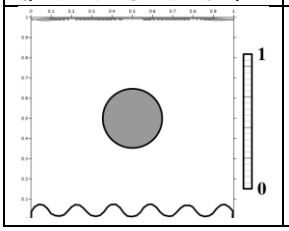	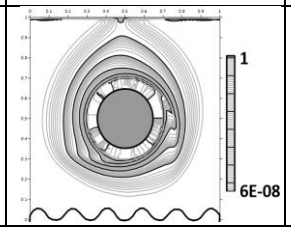	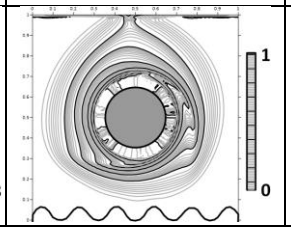	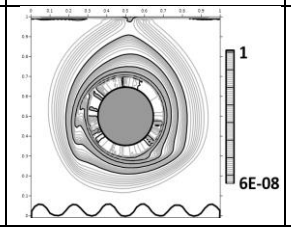	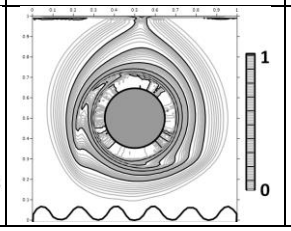	1

Fig.(10): Bejan Number behavior of Al_2O_3 – water nanofluid at various dimensionless cylinder angular velocities (Ω=0, ±3000, ±6000) and various magnitudes of HH= (0,0.25,0.5,1) from the cavity height and ϕ=0.02, Ra = 10^4, Da = 10^{-4} and R=0.15.

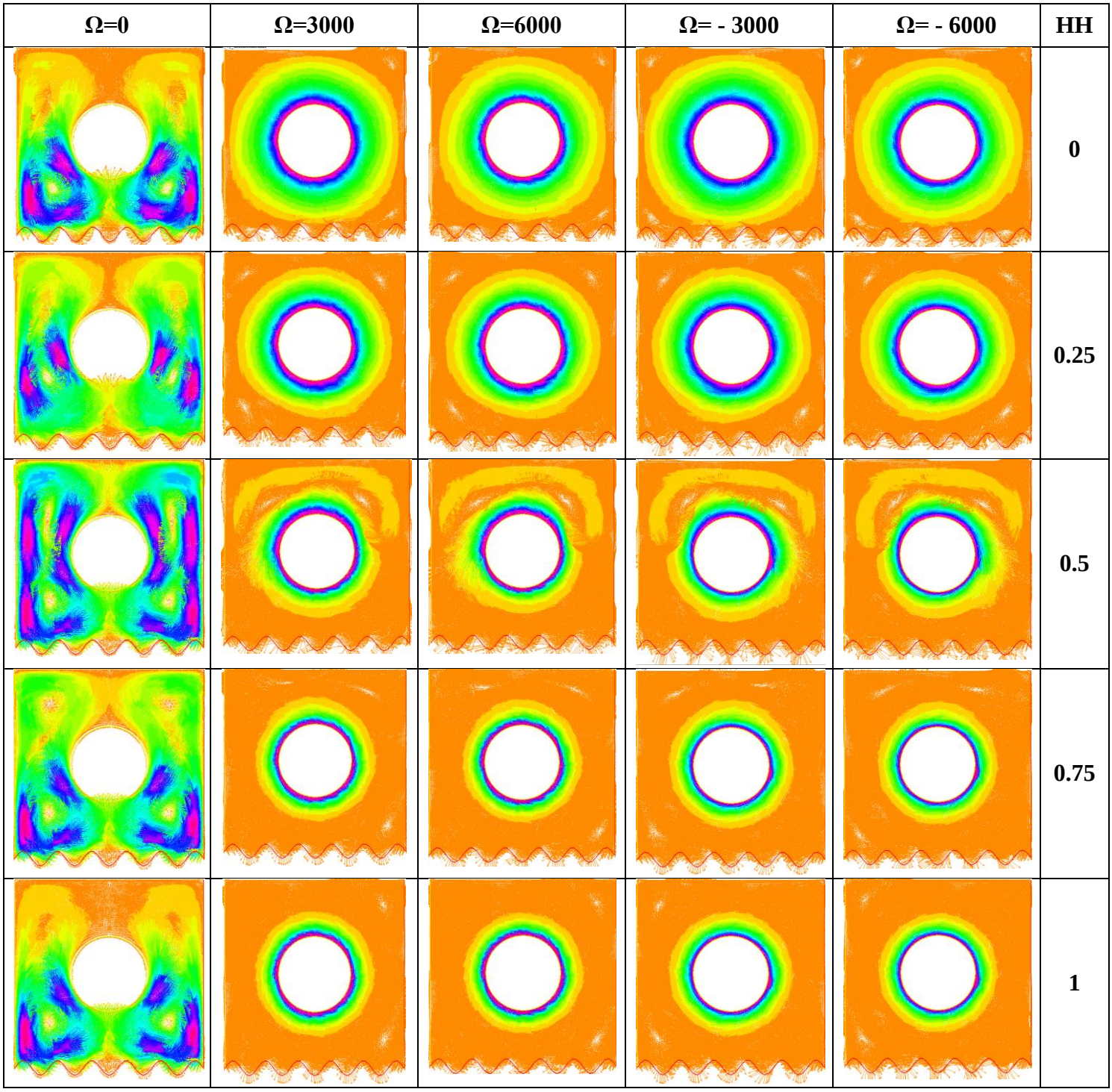

Fig. (11): The velocity vector (U, V) contour lines of Al_2O_3 – water nanofluid at various dimensionless cylinder angular velocities (Ω=0, ±3000, ±6000) and different HH= (0, 0.25, 0.5, 1) at ϕ=0.02, Ra = 10^4, Da = 10^{-4} and R=0.15.

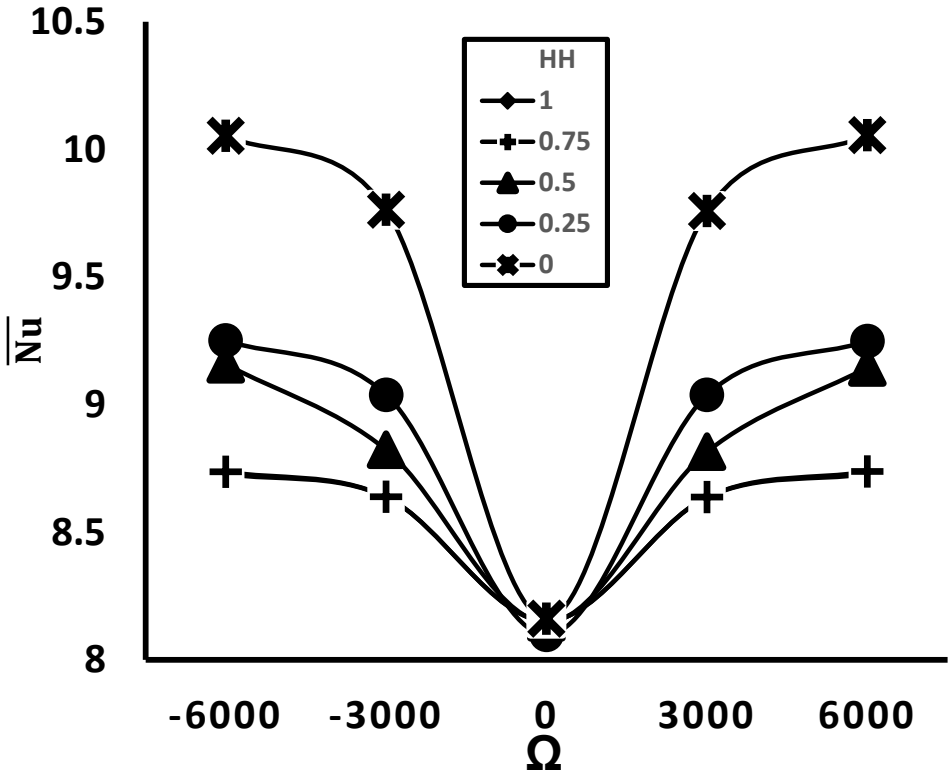

Fig. (12): Nusselt Number behavior of Al_2o_3 – water nanofluid at various dimensionless cylinder angular velocities (Ω=0, ±3000, ±6000) and various magnitudes of HH= (0,0.25,0.5,1) and ϕ=0.02, Ra = 10^4, Da = 10^{-4} and R=0.15.

Table 1. Physical features of the base fluid and nanoparticles at 25 °C (Cimpean, 2022)**.**

Physical Property	**Units**	**Base Fluid(water)**	**Al_2O_3**
Cp	J/kgK	4179	765
ρ	kg/m^3	997.1	3970
k	W/mK	0.613	40
$\beta \times 10^{-5}$	k^{-1}	21.0	0.85

Table 2. Grid sensitivity and accuracy.

elements	grid	|Ψmax|	θmax	Πmax	Nuav
672	20	0.83856	1	3.46499	9.14228
1494	30	0.84487	1	3.84464	9.78167
2598	40	0.84513	1	4.08575	10.2127
4190	50	0.84683	1	4.27515	10.5749
5928	60	0.84681	1	4.27509	10.5745

Table 3. The maximum streamfunction magnitudes with changing HH and Ω

Ω	HH				
	0	0.25	0.5	0.75	1
0	0.86	0.33	0.11	0.11	0.11
±3000	56	45	27	24	24
±6000	91	79	48	44	44

Table 4. The percentage reduction in the maximum velocity vector with increasing HH.

HH	0.25	0.5	0.75	1
Max velocity vector as a percentage to previous magnitude	75.5%	41.35%	0.78%	≈ 0.0%

REFERENCES:

Abderrahmane, A., Younis, O., Al-khaleel, M., Laidoudi, H., Akkurt, N., Guedri, K. & Marzouki, R. 2022. 2d mhd mixed convection in a zigzag trapezoidal thermal energy storage system using nepcm. Nanomaterials (basel), 12.

Abdulsahib, A. D. 2020. Mixed convection on a rotating circular cylinder in a cavity filled with nanofluid and porous media: a numerical and an experimental investigation. M.sc, university of Al-qadisiyah / college of engineering.

Aberoumand, S. & Jafarimoghaddam, A. 2016. Mixed convection heat transfer of nanofluids inside curved tubes: an experimental study. Applied thermal engineering.

Abu-Nada, E. & Oztop, H. F. 2009. Effects of inclination angle on natural convection in enclosures filled with cu–water nanofluid. International journal of heat and fluid flow, 30, 669-678.

Ahmed, A., Baig, H., Sundaram, S. & Mallick, T. K. 2019. Use of nanofluids in solar pv/thermal systems. International journal of photoenergy, 2019, 1-17.

Ahmed, F., Abir, M. A., Bhowmik, P., Deshpande, V. & Mollah, A. 2021. Thermohydraulic performance of water mixed Al_2O_3, tio2 and graphene-oxide nanoparticles for nuclear fuel triangular subchannel. Thermal science and engineering progress, 24, 100929.

Ahmed, S. Y., Jabbar, M. Y., Hamzah, H. K., Ali, F. H. & Hussein, A. K. 2020. Mixed convection of nanofluid in a square enclosure with a hot bottom wall and a conductive half- immersed rotating circular cylinder. Heat transfer, 49, 4173-4203.

Al-Amir, Q. R., Farooq Hassan Ali Alinnawi & Adnan., Q. 2019. Computational study of mixed heat convection in annular space between concentric rotating inner and wavy surface outer cylinders. Pertanika j. Sci. & technol, 0128-7680, 24.

Al-Asad, M. F., Alam, M. N., Tunç, C. & Sarker, M. 2021. Heat transport exploration of free convection flow inside enclosure having vertical wavy walls. Journal of applied and computational mechanics, 7, 520-527.

Al-Kaby, R. N., Al-Amir, Q. R., Hamzah, H. K., Ali, F. H. & Abed, A. M. 2023. Characterization of natural convection and entropy generation within a circular baffle inside two connected inclined square cavities filled with a Cu-Al_2o_3-hybrid nanofluid under thermal radiation. Journal of thermal analysis and calorimetry.

Al-Zamily, A. M. J. 2016. Analysis of natural convection and entropy generation in a cavity filled with multi-layers of porous medium and nanofluid with a heat generation. International journal of heat and mass transfer.

Alam, P., Kumar, A., Kapoor, S. & Ansari, S. R. 2012. Numerical investigation of natural convection in a rectangular enclosure due to partial heating and cooling at vertical walls. Communications in nonlinear science and numerical simulation, 17, 2403-2414.

Ali, F. H., Hamzah, H. K. & Abdulkadhim, A. 2018. Numerical study of mixed convection nanofluid in an annulus enclosure between outer rotating cylinder and inner corrugation cylinder. Heat transfer—asian research, 48, 343-360.

Ali, F. H., Hamzah, H. K., Hussein, A. K., Jabbar, M. Y. & Talebizadehsardari, P. 2020. Mhd mixed convection due to a rotating circular cylinder in a trapezoidal enclosure filled with a nanofluid saturated with a porous media. International journal of mechanical sciences, 181.

Alsabery, A. I., Ismael, M. A., Chamkha, A. J. & Hashim, I. 2018. Numerical investigation of mixed convection and entropy generation in a wavy-walled cavity filled with nanofluid and involving a rotating cylinder. Entropy, 20, 664.
Baïri, A., Zarco-Pernia, E. & García De María, J. M. 2014. A review on natural convection in enclosures for engineering applications. The particular case of the parallelogrammic diode cavity. Applied thermal engineering, 63, 304-322.
Basak, T., Kaluri, R. S. & Balakrishnan, A. R. 2012. Entropy generation during natural convection in a porous cavity: effect of thermal boundary conditions. Numerical heat transfer, part a: applications, 62, 336-364.
Bashir, A. I., Everts, M., Bennacer, R. & Meyer, J. P. 2019. Single-phase forced convection heat transfer and pressure drop in circular tubes in the laminar and transitional flow regimes. Experimental thermal and fluid science, 109, 109891.
Bellos, E., Said, Z. & Tzivanidis, C. 2018. The use of nanofluids in solar concentrating technologies: a comprehensive review. Journal of cleaner production, 196, 84-99.
Brinkman, H. C. 1952. The viscosity of concentrated suspensions and solutions. The journal of chemical physics, 20, 571-571.
Cherkasova, A. S. & Shan, J. W. 2008. Particle aspect-ratio effects on the thermal conductivity of micro- and nanoparticle suspensions. Journal of heat transfer.
Cimpean, D. S. 2022. Dynamics of colloidal mixture of Cu- Al_2O_3/water in an inclined porous channel due to mixed convection: significance of entropy generation. Coatings, 12.
Dadwal, A. & Joy, P. A. 2020. Particle size effect in different base fluids on the thermal conductivity of fatty acid coated magnetite nanofluids. Journal of molecular liquids, 303.
Das, S. K., Choi, S. U. S. & Patel, H. E. 2006. Heat transfer in nanofluids—a review. Heat transfer engineering, 27, 3-19.
Ghaffarkhah, A., Afrand, M., Talebkeikhah, M., Sehat, A. A., Moraveji, M. K., Talebkeikhah, F. & Arjmand, M. 2020. On evaluation of thermophysical properties of transformer oil-based nanofluids: a comprehensive modeling and experimental study. Journal of molecular liquids, 300.
Ghalambaz, M., Mehryan, S., Zahmatkesh, I. & Chamkha, A. 2020. Free convection heat transfer analysis of a suspension of nano–encapsulated phase change materials (nepcms) in an inclined porous cavity. International journal of thermal sciences, 157, 106503.
Ghorbani, N., Taherian, H., Gorji, M. & Mirgolbabaei, H. 2010. Experimental study of mixed convection heat transfer in vertical helically coiled tube heat exchangers. Experimental thermal and fluid science, 34, 900-905.
Hamdi, M., Sahi, A. & Ourrad, O. 2023. Mixed convection heat transfer of a nanofluid in a square ventilated cavity separated horizontally by a porous layer and discrete heat source. Archives of thermodynamics.
Hatami, M., Ali., F. H., Alsabery., A. I., Hu., S., Jing., D. & Hamzah., H. K. 2021. Mixed convection heat transfer of Sio_2-water and alumina-pao nano-lubricants used in a mechanical ball bearing. Journal of thermal engineering.
Hrairi, M., Ahmed, M. I. & Ismail, A. F. 2010. Mixed-convection heat transfer from simulated air-cooled electronic devices: experimental and numerical study. Journal of thermophysics and heat transfer, 24, 165-172.
Ingham, D. B., Bejan, A., Mamut, E. & Pop, I.2012. Emerging technologies and techniques in porous media. Springer Science and Business Media Dordrecht.

Isede, H. A. & Adeniyan, A. 2021. Mixed convection flow and heat transfer of chemically reactive drilling liquids with clay nanoparticles subject to radiation absorption. Ain shams engineering journal, 12, 4167-4180.
Jabbar, M. Y., Hamzah, H. K., Ali, F. H., Ahmed, S. Y. & Ismael, M. A. 2020. Thermal analysis of nanofluid saturated in inclined porous cavity cooled by rotating active cylinder subjected to convective condition. Journal of thermal analysis and calorimetry, 144, 1299-1323.
Khanafer, K. & Vafai, K. 2018. Applications of nanofluids in porous medium. Journal of thermal analysis and calorimetry, 135, 1479-1492.
Kumar, A. & Subudhi, S. 2021. Thermal characteristics and convection in nanofluids, springer.
Lin, j., qian, t., bechtold, p., grell, g., zhang, g. J., zhu, p., freitas, s. R., barnes, h. & han, j. 2022. Atmospheric convection. Atmosphere-ocean, 60, 422-476.
Lipiński, W., Abbasi-Shavazi, E., Chen, J., Coventry, J., Hangi, M., Iyer, S., Kumar, A., Li, L., Li, S., Pye, J., Torres, J. F., Wang, B., Wang, Y. & Wheeler, V. M. 2021. Progress in heat transfer research for high-temperature solar thermal applications. Applied thermal engineering, 184.
Mahdi, R. A., Mohammed, H., Munisamy, K. & Saeid, N. 2015. Review of convection heat transfer and fluid flow in porous media with nanofluid. Renewable and sustainable energy reviews, 41, 715-734.
Maheshwary, P. B., Handa, C. C., Nemade, K. R. & Chaudhary, S. R. 2020. Role of nanoparticle shape in enhancing the thermal conductivity of nanofluids. Materials today: proceedings, 28, 873-878.
Mehryan, S., Ghalambaz, M., Feeoj, R. K., Hajjar, A. & Izadi, M. 2020. Free convection in a trapezoidal enclosure divided by a flexible partition. International journal of heat and mass transfer, 149, 119186.
Misirlioglu, A. 2006. The effect of rotating cylinder on the heat transfer in a square cavity filled with porous medium. International journal of engineering science, 44, 1173-1187.
Özerinç, S. 2010. Heat transfer enhancement with nanofluids. Master, middle east technical university.
Prasad, P. D., Varma, S. V. K. & Kumar, R. V. M. S. S. K. 2017. Mhd free convection and heat transfer enhancement of nanofluids through a porous medium in the presence of variable heat flux. Journal of nanofluids, 6, 496-504.
Rashid, F. L., Al-Gaheeshi, A. M. R., Alhwayzee, M., Ali, B., Shah, N. A. & Chung, J. D. 2023. Mixed convection in a horizontal channel–cavity arrangement with different heat source locations. Mathematics, 11.
Roslan, R., Saleh, H. & Hashim, I. 2012. Effect of rotating cylinder on heat transfer in a square enclosure filled with nanofluids. International journal of heat and mass transfer, 55, 7247-7256.
Selimefendigil, F., Ismael, M. A. & Chamkha, A. J. 2017. Mixed convection in superposed nanofluid and porous layers in square enclosure with inner rotating cylinder. International journal of mechanical sciences, 124-125, 95-108.
Sharifi, A. H., Zahmatkesh, I., Mozhdehi, A. M., Morsali, A. & Bamoharram, F. F. 2020. Stability appraisement of the alumina-brine nanofluid in the presence of ionic and non-ionic disparents on the alumina nanoparticles surface as heat transfer fluids: quantum mechanical study and taguchi-optimized experimental analysis. Journal of molecular liquids, 319.
Shih, Y.-C. & Cheng, Y.-J. 2015. The effect of viscous dissipation on heat transfer in cavities of varying shape due to an inner rotating circular cylinder. Numerical heat transfer, part a: applications, 68, 150-173.

Sivasankaran, S. & Mallawi, F. O. M. 2021. Numerical study on convective flow boiling of nanoliquid inside a pipe filling with aluminum metal foam by two-phase model. Case studies in thermal engineering, 26.
Tiwari, R. K. & Das, M. K. 2007. Heat transfer augmentation in a two-sided lid-driven differentially heated square cavity utilizing nanofluids. International journal of heat and mass transfer, 50, 2002-2018.
Trisaksri, V. & Wongwises, S. 2007. Critical review of heat transfer characteristics of nanofluids. Renewable and sustainable energy reviews, 11, 512-523.
Trodi, A. & Benhamza, M. E. H. 2016. Particle shape and aspect ratio effect of Al_2O_3–water nanofluid on natural convective heat transfer enhancement in differentially heated square enclosures. Chemical engineering communications, 204, 158-167.
Vadász, P. 2008. Emerging topics in heat and mass transfer in porous media: from bioengineering and microelectronics to nanotechnology.
Vakili, M., Mohebbi, A. & Hashemipour, H. 2013. Experimental study on convective heat transfer of Tio_2 nanofluids. Heat and mass transfer, 49, 1159-1165.
Varol, Y., Oztop, H. F. & Pop, I. 2009. Entropy generation due to natural convection in non-uniformly heated porous isosceles triangular enclosures at different positions. International journal of heat and mass transfer, 52, 1193-1205.
Vengadesan, E. & Senthil, R. 2020. A review on recent development of thermal performance enhancement methods of flat plate solar water heater. Solar energy, 206, 935-961.
Xie, H.-Q., Wang, J.-C., Xi, T.-G. & Liu, Y. 2002. Thermal conductivity of suspensions containing nanosized Sic particles. International journal of thermophysics, 23, 571-580.
Yazdanifard, F., Ameri, M. & Ebrahimnia-Bajestan, E. 2017. Performance of nanofluid-based photovoltaic/thermal systems: a review. Renewable and sustainable energy reviews, 76, 323-352.
Zafar, M., Sakidin, H., Sheremet, M., Dzulkarnain, I., Nazar, R. M., Hussain, A., Said, Z., Afzal, F., Al-Yaari, A., Khan, M. S. & Khan, J. A. 2023. The impact of cavities in different thermal applications of nanofluids: a review. Nanomaterials (basel), 13.
Zahmatkesh, I., Sheremet, M., Yang, L., Heris, S. Z., Sharifpur, M., Meyer, J. P., Ghalambaz, M., Wongwises, S., Jing, D. & Mahian, O. 2021a. Effect of nanoparticle shape on the performance of thermal systems utilizing nanofluids: a critical review. Journal of molecular liquids, 321.
Zahmatkesh, I., Sheremet, M., Yang, L., Heris, S. Z., Sharifpur, M., Meyer, J. P., Ghalambaz, M., Wongwises, S., Jing, D. & Mahian, O. 2021b. Effect of nanoparticle shape on the performance of thermal systems utilizing nanofluids: a critical review. Journal of molecular liquids, 321, 114430.
Zarei, M. S., Khalil Abad, A. T., Hekmatifar, M. & Toghraie, D. 2022. Heat transfer in a square cavity filled by nanofluid with sinusoidal wavy walls at different wavelengths and amplitudes. Case studies in thermal engineering, 34.
Zheng, G. F., Ha, M. Y., Yoon, H. S. & Park, Y. G. 2013. A numerical study on mixed convection in a lid-driven cavity with a circular cylinder. Journal of mechanical science and technology, 27, 273-286.
Zhixiong Li, P. B., Davood Toghraie,Reza Balali Dehkordi, Masoud Afrand 2019. Mixed convection of non-newtonian nanofluid in an hshaped cavity with cooler and heater cylinders filled by a porous material: two phase approach. Faculty of engineering and information sciences, 55.